HOSTED BY

ELSEVIER

Available online at www.sciencedirect.com

ScienceDirect

Journal of Computational Design and Engineering 3 (2016) 71–90

www.elsevier.com/locate/jcde

Steel nitriding optimization through multi-objective and FEM analysis ☆

Pasquale Cavaliere, Angelo Perrone, Alessio Silvello

Department of Innovation Engineering, University of Salento, Via per Arnesano, Lecce I-73100, Italy

Received 20 April 2015; received in revised form 3 July 2015; accepted 10 August 2015
Available online 28 August 2015

Abstract

Steel nitriding is a thermo-chemical process leading to surface hardening and improvement in fatigue properties. The process is strongly influenced by many different variables such as steel composition, nitrogen potential, temperature, time, and quenching media. In the present study, the influence of such parameters affecting physic-chemical and mechanical properties of nitride steels was evaluated. The aim was to streamline the process by numerical–experimental analysis allowing defining the optimal conditions for the success of the process. Input parameters–output results correlations were calculated through the employment of a multi-objective optimization software, modeFRONTIER (Esteco). The mechanical and microstructural results belonging to the nitriding process, performed with different processing conditions for various steels, are presented. The data were employed to obtain the analytical equations describing nitriding behavior as a function of nitriding parameters and steel composition. The obtained model was validated, through control designs, and optimized by taking into account physical and processing conditions.

Keywords: Nitriding; Mechanical properties; Optimization

1. Introduction

The deep analysis of industrial processes necessitates the employment of computational multiobjective optimization tools. Optimization instruments allow integration with multiple calculation tools and post-processing tools. modeFRONTIER platform allows the organization of a wide range of software and an easy management of the entire product development process. The role of the optimization algorithm is to identify the solutions which lie on the trade-off curve, known as the Pareto Frontier. These solutions have the characteristic that none of the objectives can be improved without prejudicing another. Here, Design of Experiment (DoE) technique is used to perform a reduced number of calculations. After that, these well-distributed results can be used to create an interpolating surface. This surface represents a metamodel of the original problem and can be used to perform the optimization without computing any further analyses.

Once data has been obtained, the user can turn to the extensive post-processing features in modeFRONTIER to analyze the results.

Not so many papers are available in literature on the analysis on thermo-mechanical diffusion processes of nitriding based on Fick's laws model. In the present paper the behavior of nitriding process, performed on different steels (40 different materials) in a broad range of processing parameters (600 experimental conditions), is analyzed. The study leads to the description of the nitriding effect on the steel structures and mechanical properties. In [1] the authors give a mathematical description to predict the nitrogen contents as well as residual stresses and distortions after nitride quenching. The model was implemented in finite element calculations in order to identify the concentration profiles. They concluded that the interactions between diffusion of nitrogen also need to be established. In general, the hardening of steels during nitriding process is due to the N-based compounds precipitation [2]. The precipitation sequence is also strongly influenced by the compounds time formation. Several nitrogen mass transfer mechanisms have been proposed to describe the nitrides precipitation process. In [3], the authors analyzed the nitriding process by employing the Mullins–Sekerka equations on the interface separating a growing nitride layer in pure iron. They showed that a plane interface is unconditionally stable due to the favorable

☆ Peer review under responsibility of Society of CAD/CAM Engineers.

http://dx.doi.org/10.1016/j.jcde.2015.08.002

Nomenclature

T_H	heat treatment temperature
N_p	nitrogen potential
T_N	nitriding temperature
t_N	nitriding time
N_*xxx*	nitrogen concentration at *xxx* μm from the surface
ε_s	distance from the surface of the starting point of ε phase
ε_f	distance from the surface of the ending point of ε phase
γ'_s	distance from the surface of the starting point of γ' phase
γ'_f	distance from the surface of the ending point of γ' phase
Hv_*xxx*	microhardness at *xxx* μm from the surface
σ_*xxx*	residual stresses at *xxx* μm from the surface

combination of the Gibbs–Thomson effect, and of the concentration fields. This result is specific to the nitriding configuration where the net flux of nitrogen is in the growth direction. The influence of compositional and misfit generated stresses on the morphological stability has been discussed qualitatively. For these reasons, in the present paper, a large attention vas devoted to the measurement and the control of compound layers and on their effect on mechanical properties. Other authors described results of simulations of diffusional process of nitrogen on pure iron. They underline the effect of nitriding potential of NH_3–H_2 atmosphere on microstructural constitution and growth kinetics of nitride layers. They demonstrate that both microstructural nature and thicknesses of nitrided layers as well as the nitrogen profile within the formed phases during gas nitriding can be predicted [4,5]. In [6], a generalized Wagner diffusion model was used to analyze the layer formation and growth in definite experiments on plasma nitriding of pure iron. The model is able to predict the compound layer composition. It can be used as a method for calculation of the effective diffusion coefficients in the first sublayer of the compound zone. The thickness of the compound layer and the diffusion zone as well as their phase composition and the consequent mechanical properties depends on the nitriding temperature and time. It also depends on the nitrogen activity of the medium in which the nitriding process is taking place. In addition such chemical–physical processes depend on the state of the material before nitriding [7]. For this reason, in the present multi-objective optimization analysis the state of the material (in particular the heat treatment temperature) before nitriding was taken into account. In [8] the authors modeled the nitrogen decomposition on the steel surface as a consequence of processing parameters. In [9] the authors evidence the nitride layers formation in high temperature gas nitriding of stainless steel. In [10,11] other authors underline the nitriding properties of steel after treatment at high temperatures up to 1050 °C. In [12] the authors model the process through finite element analyses by employing microstructural data obtained from X-rays diffraction measurements. The same methods for microstructural evolution monitoring are described in [13]. The method is largely

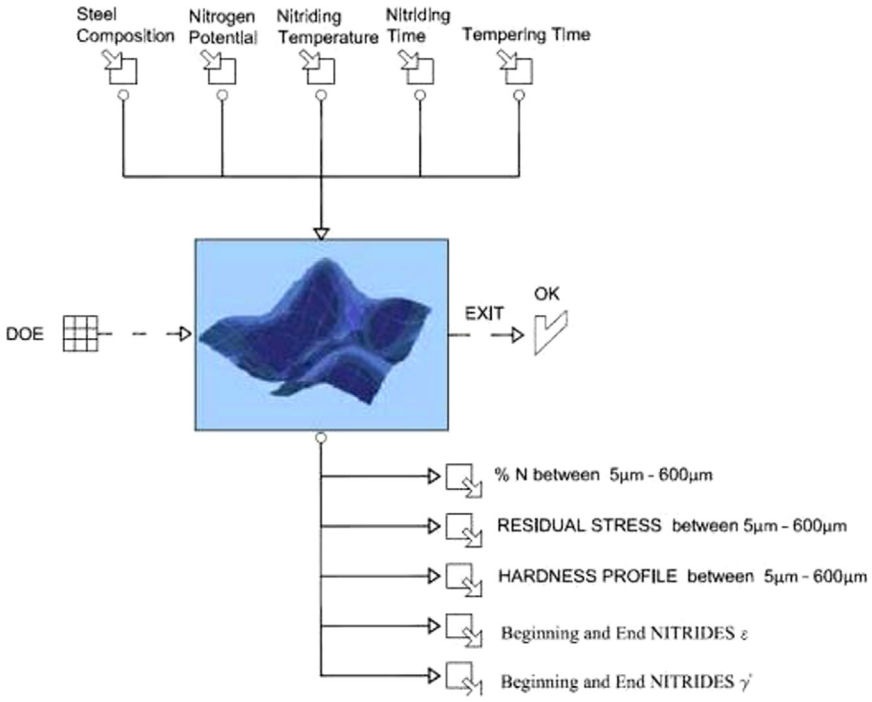

Fig. 1. Workflow of analysis describing the input–output correlation.

Table 1
Composition of some of the steels analyzed in the present study.

Steel	C (%)	Si (%)	Cu (%)	Mn (%)	Cr (%)	Ni (%)	Mo (%)	Al (%)	Ti (%)	V (%)	Nb (%)	S (%)	Co (%)	W (%)	N (%)	P (%)
AISI1020	0.2	0.8	0	0.9	13	0	0	0	0	0	0	0.02	0	0	0	0.01
15CrMoV5-9	0.05	0.6	0.8	1.1	18.3	8.5	0	0	0.01	0	0	0.01	0	0	0	0.01
AISI5115	0.16	0.28	0	1.15	0.95	0	0	0	0	0	0	0.01	0	0	0	0.01
25CrMo20	0.25	0	0	0	5	0	0.2	0	0	0	0	0.01	0	0	0	0.015
31CrMo12	0.3	0.3	0	0.7	3.2	0	0.35	0	0	0	0	0.01	0	0	0	0.01
32CrMoV13	0.28	0.35	0	1.54	0.26	0	0	0	0	0.11	0	0.012	0	0	0	0.015
34CrNiMo6	0.38	0.26	0	0.7	0.8	0.7	0.22	0	0	0	0	0.01	0	0	0	0.02
34CrAlNi7	0.34	0	0	0	1.7	1	0.2	1	0	0	0	0.01	0	0	0	0.01
39NiCrMo3	0.4	0.3	0	0.7	1	1	0.2	0	0	0	0	0.02	0	0	0	0.01
42CrMo4	0.38	0.4	0	0.65	1.2	0	0.15	0	0	0	0	0.015	0	0	0	0.015
50VCr11	0.45	0.5	0	1	11	0.7	0	0	0	0.3	0	0.03	0	0	0	0.03
AISI304	0.05	0.56	0.8	1.12	18.3	8.5	0	0	0.01	0	0	0.012	0	0	0	0.013
AISI316L	0.07	1.00	0	2.00	17.50	12.00	2.00	0	0	0	0	0.03	0	0	0	0.05
X6Cr17	0.08	0	1	1	17	0	0	0.3	0	0	0	0.015	0	0	0	0.04
AISI410	0.12	1	0	1.5	13	0.75	0	0	0	0	0	0.015	0	0	0	0.04
AISI431	0.2	0.8	0	0.8	16	2	0	0	0	0	0	0.02	0	0	0	0.015
AISI4140	0.4	0.5	0	1.1	1	0	0.2	0	0	0	0	0.04	0	0	0	0.035
AISI4340	0.4	0.25	0	0.7	0.8	1.85	0.25	0	0	0	0	0.02	0	0	0	0.015
AISI7140	0.42	0.3	0	0.55	1.6	0	0.38	1	0	0	0	0	0	0	0	0
H10	0.36	0.39	0	0.32	2.96	0	2.86	0	0	0.41	0	0.002	0	0	0	0.03
H11	0.42	1.22	0	0.49	5.1	0	1.27	0	0	0.44	0	0	0	0	0	0
H12	0.36	0.87	0	0.43	5	0	1.7	0	0	0.33	0	0.01	0	1.15	0	0.01
H13	0.37	1	0	0.45	5.33	0.08	1.24	0	0	0.83	0	0.015	0	0	0	0.01

described in [14,15] with many experimental evidences. In [16–18] the authors analyze the microstructural evolution of nitride layers through X-ray diffraction and model the nitriding behavior of H13 tool steel through finite method. In [19,20] the authors modeled the nitriding behavior through the analyses of compound layers thickness. The aim of the present paper is the complete experimental–numerical analyses of nitriding process. The model is developed to design a platform capable of analyzing the best conditions to reach high performances of nitride components. In addition, it can be used to design a specific steel capable to be nitride in order to reach specific performances under fixed processing conditions. The strength of the analyses is due to the large quantity of data employed to develop the proposed model.

2. Experimental procedure

2.1. Samples preparation and characterization

Steel cylindrical samples of 100 mm in diameter were nitrided by varying the nitrogen potential, nitriding temperature and time. Nitriding process was performed in a laboratory furnace equipped with a sensor capable to perform measurements of nitrogen potential in the furnace atmosphere. The sensor is sensible to hydrogen concentration that varies with ammonia dissociation. In this way it is possible to control the ammonia flux in order to fix the nitrogen potential. Compositional measurements were performed through EDX microanalyses in a Zeiss EVO40 SEM. Residual stresses and nitrides thickness layers measurements were performed through X-ray diffraction by using a Rigaku Ultima+diffractometer by employing Hall–Williamson plotting. Hall–Williamson method [21] is based on the principle that the lattice size broadening and strain broadening vary quite differently with respect to Bragg angle. By scannning a surface with X-rays and measuring the peaks shift of the spectrum, residual strains (and residual stresses) can be measured. Samples were cut

Table 2
Example of nitriding input parameters employed in the present study.

Steel	T_H (°C)	N_p (%)	T_N (°C)	t_N (h)
AISI1020	550	12	350	0.5
15CrMoV5-9	433	26	430	179
AISI5115	170	6	510	50
25CrMo20	600	3	520	1
31CrMo12	570	3	520	30
32CrMoV13	600	1.5	550	100
34CrNiMo6	571	14.4	510	176
34CrAlNi7	600	1.2	500	3
39NiCrMo3	552	5.6	1180	40
42CrMo4	600	1.3	550	6.5
50VCr11	420	3	520	1
AISI304	20	10	580	5.5
AISI316L	20	35	500	5
X6Cr17	600	15	450	24
AISI410	720	3	520	20
AISI431	799	20.8	925	128
AISI4140	560	6	550	14
AISI4340	588	11.4	1185	143
AISI7140	570	12.4	930	124.5
H10	600	15	510	12
H11	486	21	1200	150.5
H12	600	15	580	8
H13	540	17.4	750	33.5

Table 3
Example of output results measured after nitriding.

Steel	N_0 (%)	N_200 (%)	ε_s (μm)	ε_f (μm)	γ'_s (μm)	γ'_f (μm)	Hv_0	Hv_200	σ_0 (MPa)	σ_100 (MPa)
AISI1020	0.2	0	0	2	0	2	340	290	−70	−65
15CrMoV5-9	3	0.1	0	20	0	130	870	520	−130	−310
AISI5115	3	0.4	0	60	0	210	750	600	−110	−310
25CrMo20	0.4	0	0	5	0	25	450	310	−50	−160
31CrMo12	3	0.2	0	25	0	160	950	800	−400	−600
32CrMoV13	1.4	1.4	0	30	0	210	870	720	−350	−450
34CrNiMo6	6	0.7	0	170	0	510	990	560	−140	−250
34CrAlNi7	1	0	0	5	0	70	850	400	−260	−280
39NiCrMo3	3	0	0	5	0	25	620	340	−140	−380
42CrMo4	1.3	0.3	0	25	0	360	700	500	−50	−70
50VCr11	1.3	0	0	40	0	45	1100	380	−80	−170
AISI304	10	0	0	32	0	75	1280	200	−200	−120
AISI316L	21	0	0	20	0	40	1100	1060	−280	−200
X6Cr17	9	0	0	30	0	45	1220	260	−90	−170
AISI410	2	0.2	0	65	0	180	1200	320	−400	−540
AISI431	1.2	0	0	6	0	21	590	230	−140	−460
AISI4140	4	0.6	0	80	0	320	750	520	−130	−160
AISI4340	7	0	0	7	0	14	470	210	−140	−390
AISI7140	2	0	0	15	0	90	640	210	−110	−170
H10	14	0.1	0	20	0	140	1100	510	−230	−420
H11	11	0	0	30	0	90	840	140	−180	−490
H12	8	0	0	18	0	170	1070	300	−200	−540
H13	11	0	0	2	0	11	970	280	−290	−620

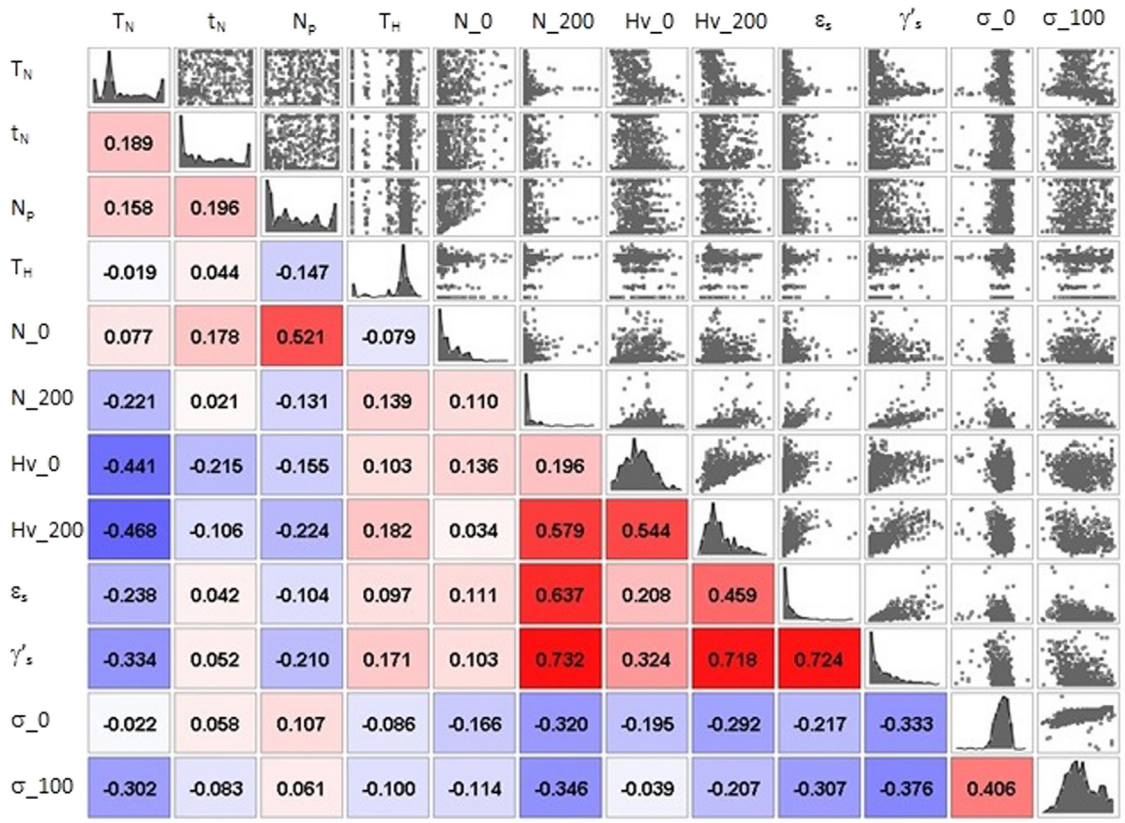

Fig. 2. Correlation matrix describing the different weights between input and output analyzed in the present study.

along the center section, grinded and polished, then the residual stresses were measured from the surface to the bulk. Microhardness was measured by employing a Vickers indenter with a 1000 gf load for 15 s.

2.2. Database construction

The employed multidisciplinary and multi-objective software is written to allow easy coupling to any computer aided engineering (CAE) tool. It enables the pursuit of the so-called "Pareto Frontier": it is the best trade-off between all the objective functions. The advanced algorithms within can spot the optimal results, even conflicting each other or belonging to different fields. The more accurate the analysis is, the more the complexity of the design process increases. modeFRONTIER® platform allows the managing of a wide range of software and an easy overview of the entire product development process. modeFRONTIER's optimization algorithms identify the solutions which lie on the trade-off Pareto Frontier: none of them can be improved without prejudicing another. In other words the best possible solutions are the optimal solutions. An attempt to optimize a design or system where there is only one objective usually entails the use of gradient methods where the algorithms search for either the minimum or the maximum of an objective function, depending on the goal. One way of handling multi-objective optimization is to incorporate all the objectives (suitably weighted) in a single function, thereby reducing the problem to one of single objective optimization again. This technique has the disadvantage, however, that these weights must be provided a priori, which can influence the solution to a large degree. Moreover, if the goals are very different in substance (for example cost and efficiency) it can be difficult, or even meaningless, to try to produce a single all-inclusive objective function.

True multi-objective optimization techniques overcome these problems by keeping the objectives separate during the optimization process. It should be kept in mind that in cases with opposing objectives (an example would be to minimize a beam's weight, and also its deformation under load) there will frequently be no single optimum, since any solution will be a compromise. The role of the optimization algorithm is then to

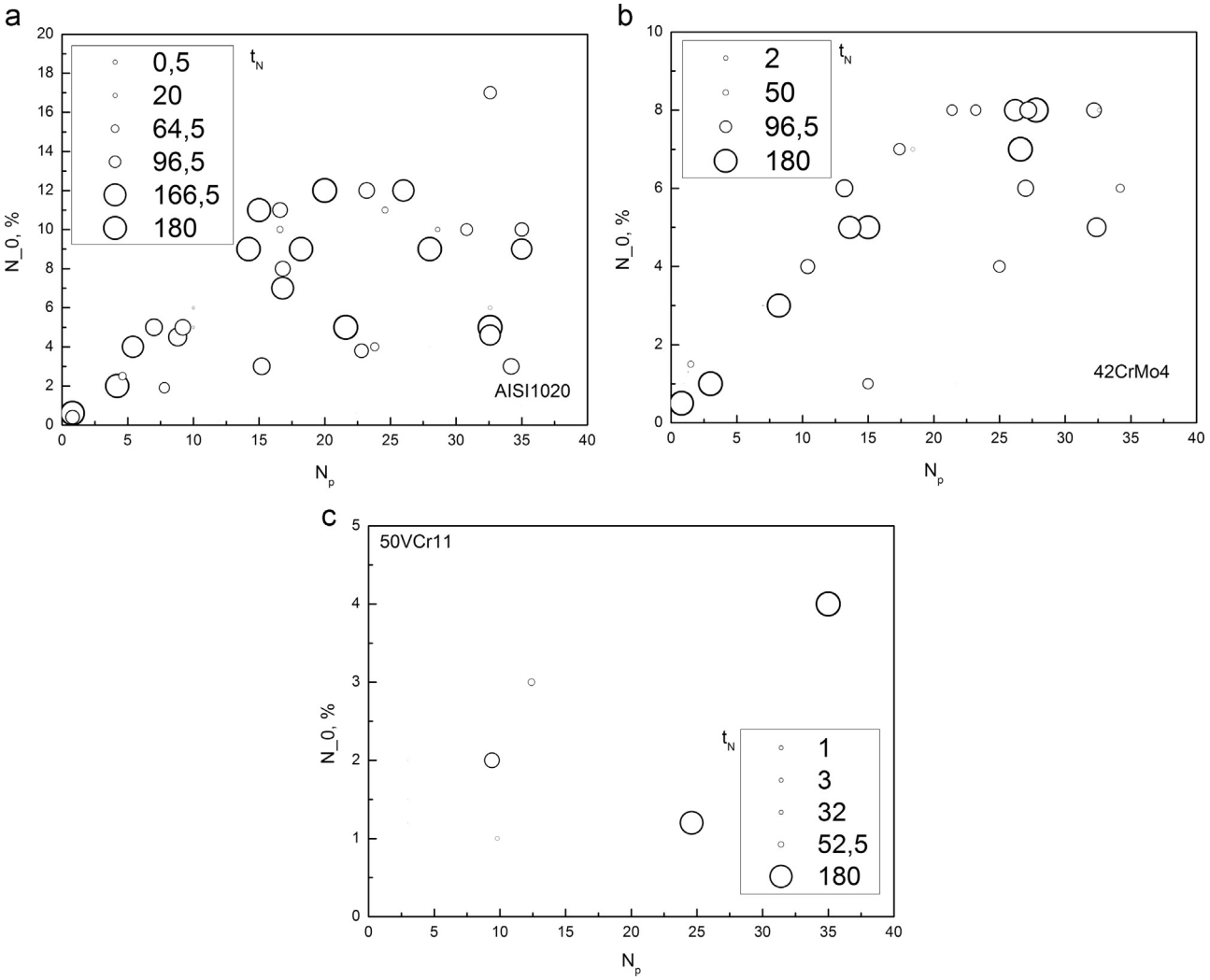

Fig. 3. Nitrogen concentration on the surface as a function of nitrogen potential and nitriding time for different steels for AISI1020 (a), 42CrMo4 (b), and 50VCr11 (c).

identify the solutions which lie on the trade-off Pareto Frontier. These solutions all have the characteristic that none of the objectives can be improved without prejudicing another.

The progresses of high performance computing offer the availability of accurate and reliable virtual environments to explore several possible configurations. In real case applica-

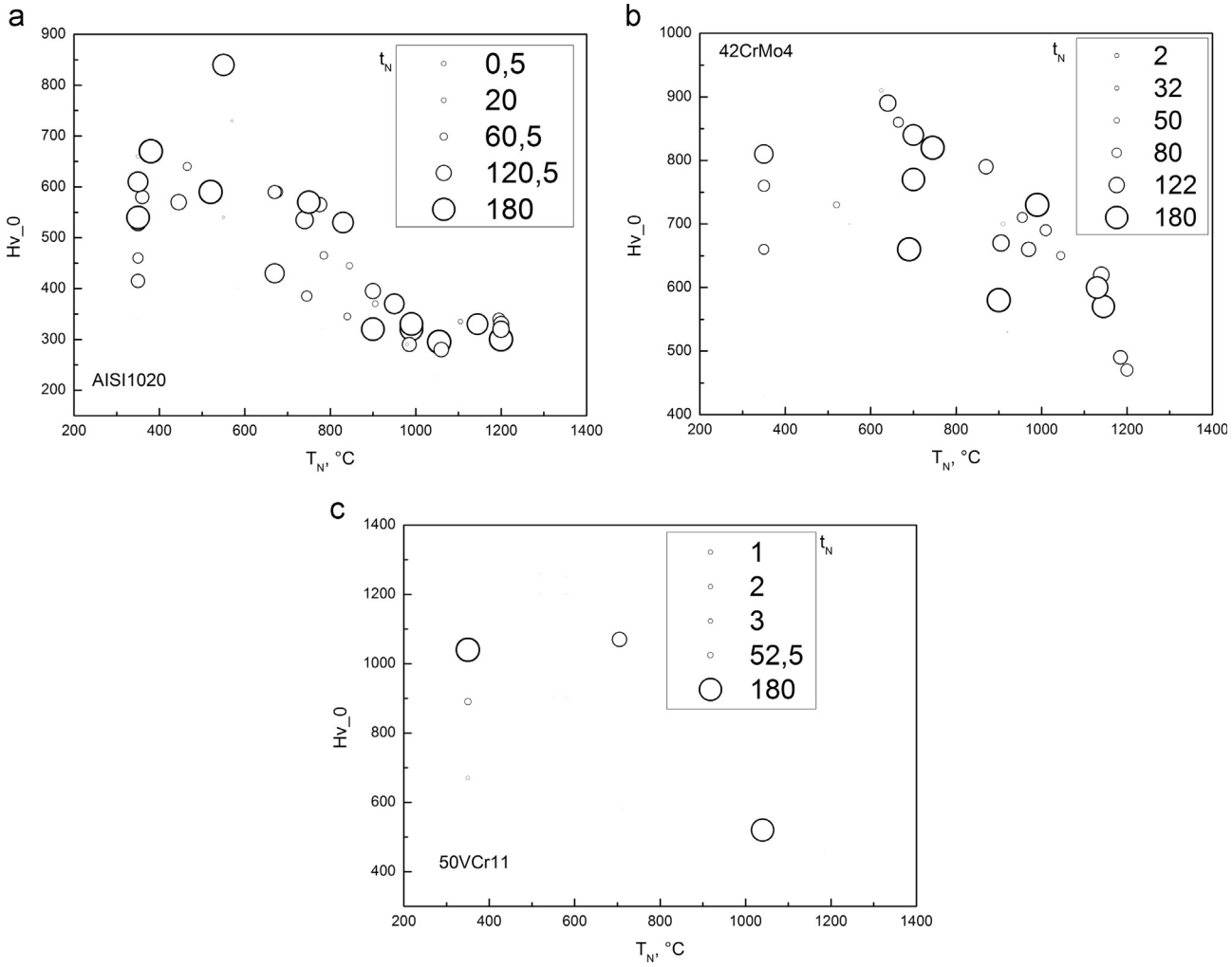

Fig. 4. Microhardness on the surface as a function of nitriding temperature and nitriding time for different steels for AISI1020 (a), 42CrMo4 (b) and 50VCr11 (c).

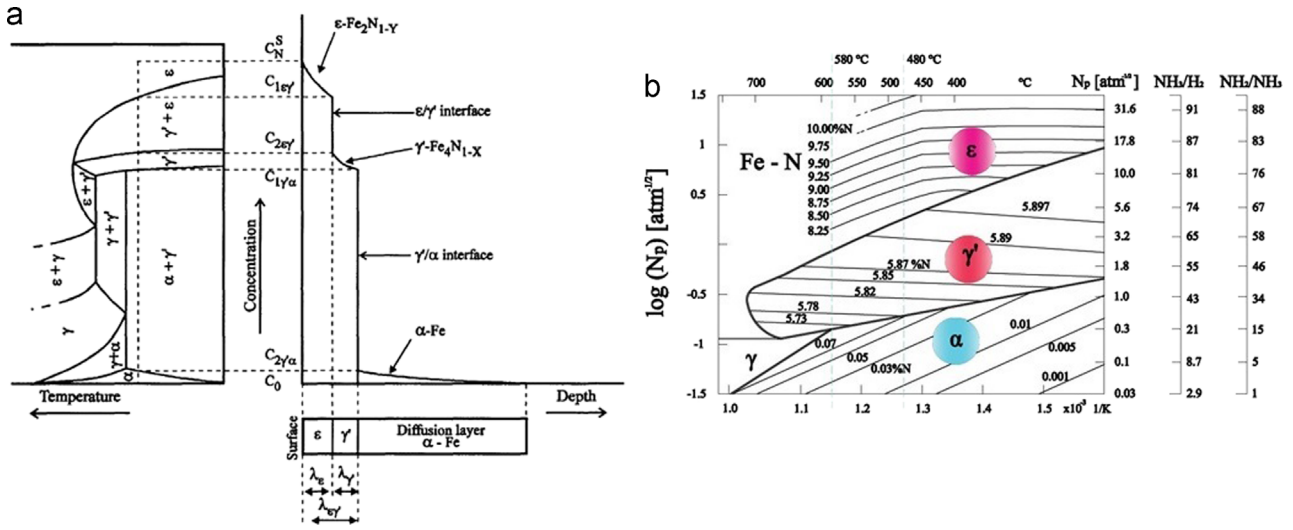

Fig. 5. Different hardening phases as a function of temperature and percentage of different elements in the Fe–N diagram (a) and Leher diagram (b) [1].

tions, it is not always possible to reduce the complexity of the problem and obtain a model that can be solved quickly. Usually every single simulation can take hours or even days. In these cases, the time to run a single analysis makes running more than a few simulations prohibitive and some other smart approaches are needed. These factors lead to a Design of Experiment (DOE) technique to perform a reduced number of calculations. After that, these well-distributed results can be used to create an interpolating surface. This surface represents a meta-model of the original problem and can be used to perform the optimization without computing any further analyses.

Once data have been obtained, whether from an optimization or DOE, or from data importation, the user can turn to the extensive post-processing features in modeFRONTIER to analyze the results. The software offers wide-ranging toolbox, allowing the user to perform sophisticated statistical analysis and data visualization. It provides a strong tool to design and to analyze experiments, it eliminates redundant observations and reduces the time and the resources to make experiments. Design of Experiments (DOE) is a methodology that maximizes the knowledge gained from an experimental campaign. Design of Experiments (DOE) is generally used in two ways. First of all, the use of DOE is extremely important in experimental settings to identify which input variables most affect the experiment being run. Since it is frequently not feasible in a multi-variable problem to test all combinations of input parameters, DOE techniques allow the user to extract as much information as possible from a limited number of test runs. However, if the engineer's aim is to optimize his design, he will need to provide the optimization algorithm with an initial population of designs from which the algorithm can "learn". In this setting, the DOE is used to provide the initial data points.

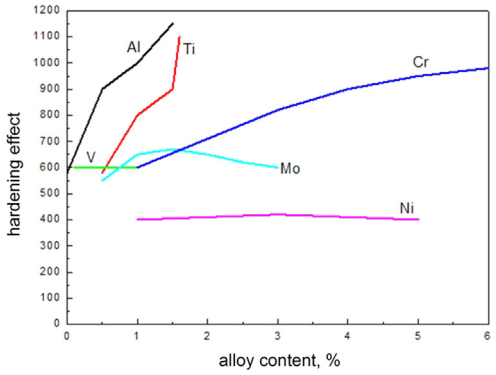

Fig. 6. Hardening effect of the different alloying elements percentage.

Exploration DOEs are useful for getting information about the problem and about the design space. They can serve as the starting point for a subsequent optimization process, or as a database for response surface (RS) training, or for checking the response sensitivity of a candidate solution.

Starting from a database built with experimental results, computational models were developed (virtual n-dimensional surfaces) able to reproduce at best the actual process. Through such analysis it was possible to optimize the output variables (% N, residual stress, beginning and end nidrides ε, beginning and end nidrides γ'). The method used for the creation of meta-models to simulate the actual process through the use of physical laws with appropriate coefficients to be calibrated was that of the response surfaces (RS). This method consists of creating n-dimensional surfaces that are "trained" on the basis of actual input and output. These surfaces trained on a large experimental data can give the output numbers that reflect the real process of nitriding. The experimental design consists of 600 input and output obtained from experimental data. To train

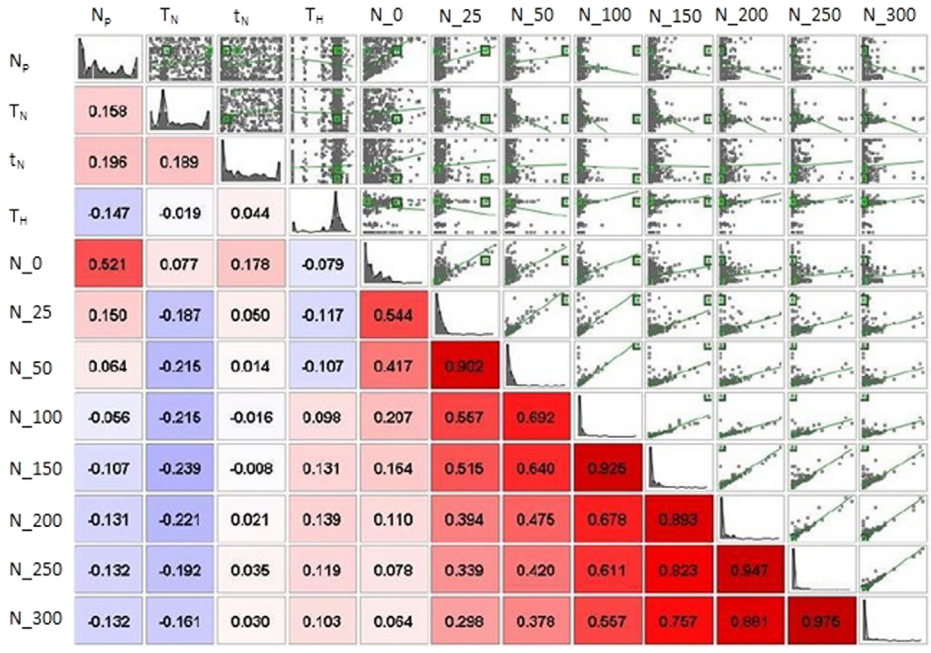

Fig. 7. Correlation matrix describing the different weights between input parameters and nitrogen concentration at different distances from the surface.

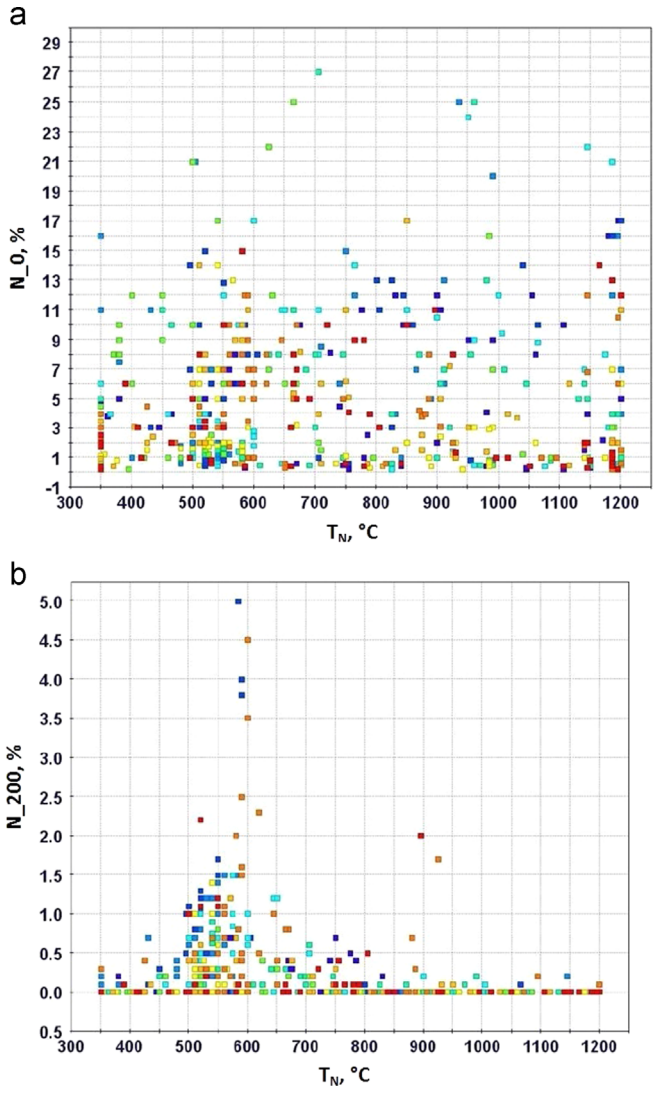

Fig. 8. Scatter charts describing the nitrogen concentration as a function of nitriding temperature on the surface (a) and at 200 μm thickness (b).

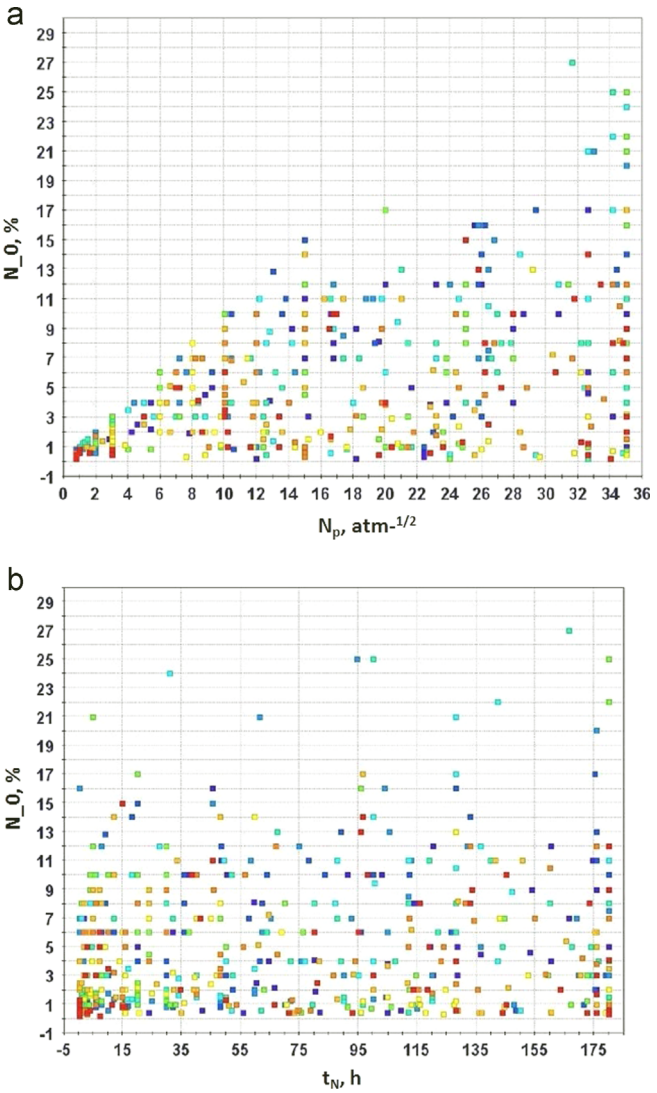

Fig. 9. Nitrogen concentration on the surface as a function of nitrogen potential (a) and nitriding time (b).

the virtual surface in the training phase they included 580 experimental design inputs and outputs. We used he remaining 20 in the design validation phase.

The computational details were largely described by the authors in [22].

The nitriding process through the analysis performed by Mode FRONTIER is summarized in the Workflow of Fig. 1.

The workflow is divided into data flow (solid lines) and logic flow (dashed lines) that have the computer node as their common node. Here physical and mathematical functions representing the nitriding process are introduced. In the data flow all input parameters optimized in the numerical simulations are included:

- steel composition,
- nitrogen potential,
- nitriding temperature,
- nitriding time,
- tempering time,

And those output:

- % nitrogen hardened layer between 5 μm and 600 μm of distance from the surface of the sample.
- Residual stress between 5 μm and 600 μm of distance from the surface of the sample.
- Hardeness stress profile between 5 μm and 600 μm of distance from the surface of the sample.
- Beginning and end nidrides ε.
- Beginning and end nidrides γ'.

2.3. Multi-objective analyses

The output variables define a multi-goal analysis and have been minimized taking into account some constraints or

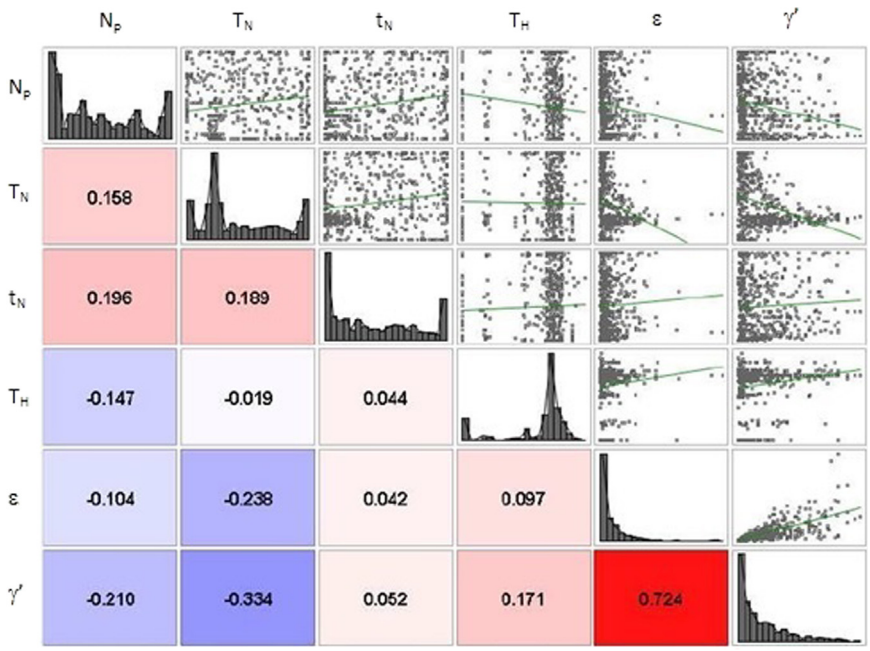

Fig. 10. Correlation matrix describing the hardening phases thickness dependence on the nitriding input parameters.

limitations typical of the actual process. At this stage the nodes that make up the logic flow of numerical analysis are defined. The first node is the DoE, which is the set of different designs reproducing different possible working conditions. It means creating a set number of designs that will be used by the scheduler (the node where the best algorithm is introduced) for the optimization. Depending on how this space is filled, the designs, defined by the scheduler, are more or less truthful. Therefore the choice of the DoE is to be assessed correctly.

Generally, in this kind of analysis, the heart of the optimization is represented by a series of equations of chemical and physical nature of a given resolution to get the desired output. In the present case, all this information is not clear, due to the complexity of the process and so it was chosen to employ the methodology of response surfaces. Optimization software allows the following of different kinds of RS. For each output variable to be minimized it is necessary to create a response surface. The analysis starts from a database built with data of operating conditions of the sintering plants obtained from experimental measurements. The database is built by introducing the input parameters, the corresponding output for each working condition and the physical correlations between the different conditions (Tables 1 and 2).

The steel compositions and the nitriding input parameters examples, performed on the cyclindrical samples, are summarized in the following tables.

3. Results and discussion

The output results, corresponding to the steel compositions and input parameters previously shown, are listed in Table 3. As a general behavior microhardness in steels is strongly dependent on nitriding temperature; on the contrary they are differently dependent on the nitrogen potential as a function of steel composition and nitriding time.

Of the 600 starting designs, 580 were used to generate meta-models, while 20 designs were employed as designs of control to verify the affordability of the response surfaces. The choice of these 20 was taken in order to get the right information on the entire range of existence of the output variables.

In the present study response surfaces (RS) that are best suited to deal with a multi-objective optimization were obtained. The next step is to evaluate the surface performance and use them as a node operator in our Work Flow. The available tools are the ones offered by modeFRONTIER, such as RS distance, the RS residual and RS function plot. Initially the tool RS distance was employed. It allows to graphically assess the distance between the real values, provided by the database, and those generated by the virtual meta-model. The virtual profile is very close to that of the actual design.

The employment of the so-called “correlation matrix” is fundamental. It allows to recognize how much the different variables are correlated between them. The parameters are strongly correlated if the corresponding value in the table is distant from zero in a range between -1 and 1; if the value is 1 the parameters are directly correlated, while if the value is -1 the parameters are inversely correlated. An example for the present study is given in Fig. 2. From the matrix it is also possible to observe the different weights of all the parameters; the more the value differs from 0 the more it influences the corresponding variable.

The nitrogen concentration, material hardness and residual stresses at different distances from the surface (0 and 200 μm for nitrogen and hardness, 0 and 100 μm for residual stresses); the ε and γ' nitrides thickness layers dependences on nitriding parameters are shown. Nitrogen concentration on the surface

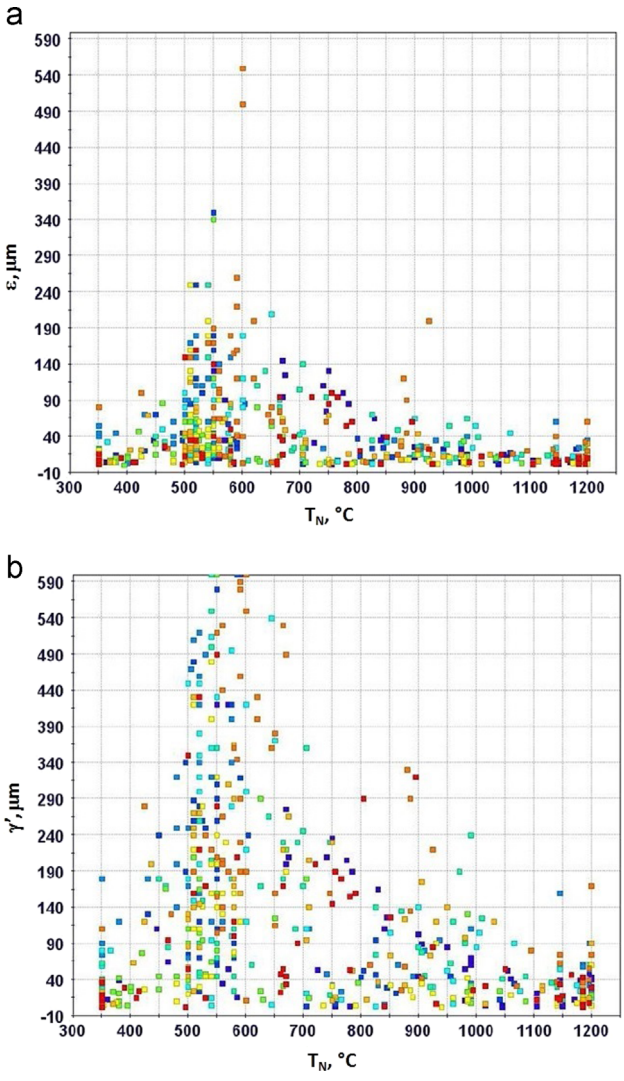

Fig. 11. Hardening phases thickness as a function of the nitriding temperature: ε in (a) and γ' in (b).

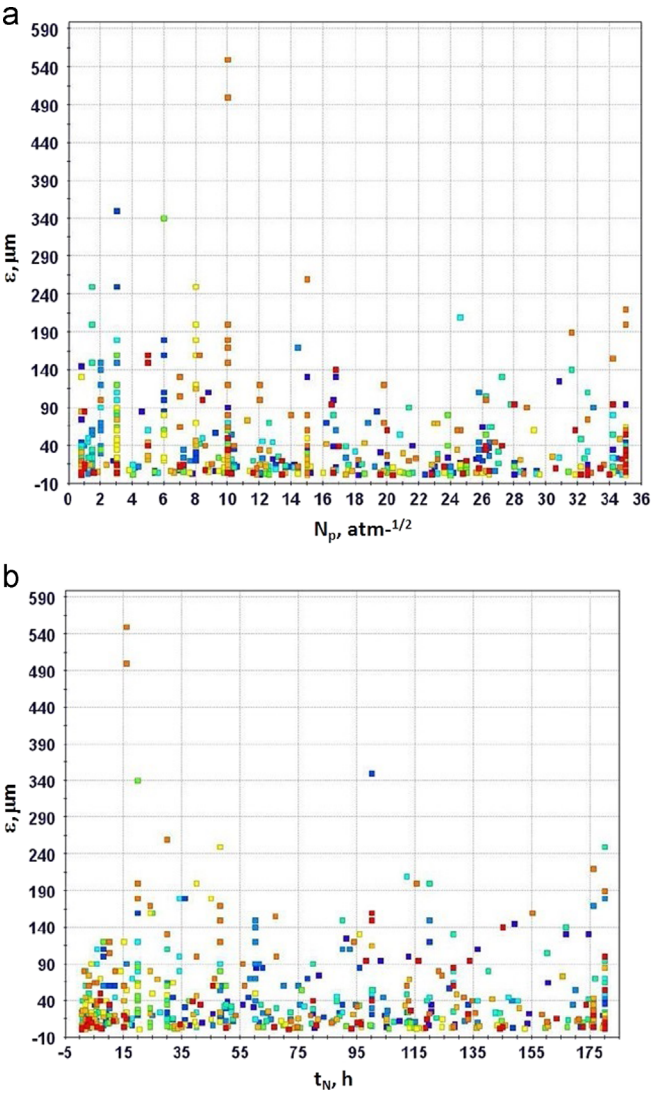

Fig. 12. ε Phase thickness as a function of nitrogen potential (a) and nitriding time (b).

(N_0) is strongly dependent on nitrogen potential and on nitriding time. An example of bubble graph for AISI1020, 42CrMo4, 50VCr11 and all the collected data is given in Fig. 3.

Fig. 3a shows that nitrogen concentration on the samples surface increases with nitrogen potential and temperature increase for AISI1020. An example of linear increase is shown for 42CrMo4 steel (Fig. 3b). A non-linear dependence is observed for other steels such as 50CrV11 (Fig. 3c). The nitrogen concentration at 0.2 mm from the surface (N_200) is directly dependent on heat treating temperature before nitriding. It is inversely proportional to nitriding temperature and nitriding potential. The surface hardness (Hv_0) is dependent strongly on nitriding temperature, then on nitriding time (Fig. 4). A linear dependence on nitriding temperature and time is underlined for AISI1020 (Fig. 4a); for 42CrMo4 (Fig. 4b) and for 50CrV11 (Fig. 4c).

Microhardness, at 0.2 mm from the surface (H_200), is dependent on the same parameters with almost the same weight. Surface residual stresses (σ_0) are dependent on the nitrogen potential. Residual stresses, at 0.1 mm from the surface (σ_100), are dependent on nitriding temperature and heat treating temperature. Residual stresses are strongly a function of the compound layers formed during diffusion.

3.1. Analytical model

Nitriding process leads to the steel hardening thanks to the diffusion of nitrogen in the interstitial sites of iron. The phenomenon produces the precipitation of high hardness nitrides. Nitrides layers are generally:

- Surface zone (5–30 µm) with varying portions of Feγ' Fe_4N (face centered cubic ductile phase) and $Fe_{2-3}N$ (HCP) more brittle but with very good wear properties.
- Another zone (0.05–0.8 mm) that results a solid solution of nitrogen in the ferrite with the presence of nitrides and

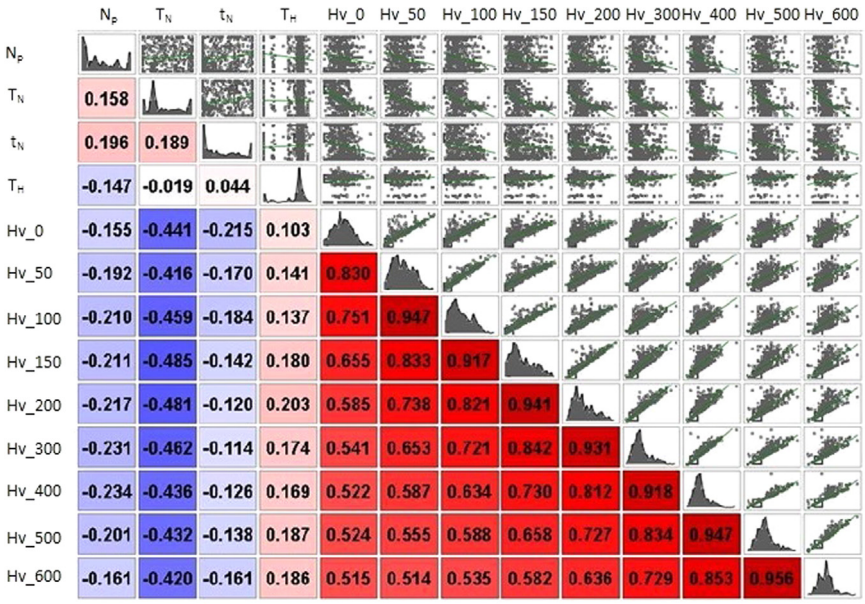

Fig. 13. Correlation matrix describing the different weights between input parameters and hardness at different distances from the surface.

carbo-nitrides (CrN, AlN, TiN,…) is in the form of very fine reinforcing particles (Fig. 5).

The analytical model relative to the equations employed to solve Fick's laws to be implemented in the finite element code is largely described in [2].

In the present study, the hardening effect of the alloying elements has been evaluated through the implementation of the equations relating the hardness increase as a function of alloying elements percentage as shown in Fig. 6.

In the present approach, the evaluation of the dependence on the main input parameters on the nitrogen diffusion has been analyzed. The scatter matrix of the nitrogen diffusion as a function of input parameters is shown in Fig. 7.

In the surface layers, a linear dependence on nitrogen potential can be underlined. The dependence tends to zero after 300 μm. In the inner layers, a linear inverse proportionality with the nitriding temperature can be observed. In order to correlate the local nitrogen diffusion to the nitriding parameters, it is useful to employ scatter charts relative to single points. In Fig. 8 the nitrogen concentration on the surface and at a thickness of 200 μm are described.

The optimal nitriding temperature, for the maximum concentration of nitrogen on the surface, is around 700 °C; the optimal nitriding temperature, for the maximum concentration at 200 μm from the surface, is 600 °C.

Nitrogen concentration on the surface is linearly dependent on the nitrogen potential while it seems less dependent on the nitriding time (Fig. 9). The points in different colors belong to different processing conditions and steels.

The layer's thickness of the different phases was monitored. The corresponding scatter matrix dependence is shown in Fig. 10.

Hardening phases thicknesses are non-linearly dependent (in particular with regard to the nitriding temperature) on the input parameters. A local approach better describes these conditions. The singular hardening phases (CrN, AlN, TiN,…) were not identified; in the present paper, thicknesses of the different layers were evaluated through the coupled variation in hardness and residual stresses. The ε and γ' thicknesses as a function of nitriding temperature are shown in Fig. 11.

ε and γ' reach their maximum thickness for a nitriding temperature around 600 °C. Their thickness increases with increasing the nitrogen potential up to 10 $atm^{-1/2}$, then a decrease is observed. Hardening phases thickness shows a maximum for a nitriding time around 15–20 h (Fig. 12).

The experimental results of the present study demonstrated that the nitrogen potential influences the maximum surface hardness values. On the contrary, nitrogen potential does not influence the hardness profile; it is strongly influenced by the steel composition. The corresponding scatter matrix shows the correlation between the nitriding parameters and the hardness profile (Fig. 13).

It is difficult, in such a case, giving some linear dependence of the hardness profile on the nitriding processing conditions. By taking into account a local approach we can observe that the surface hardness increases with the increase of nitrogen potential for low values, then it decreases with the increase of nitrogen potential (Fig. 14a). The surface hardness linearly increases with increasing the nitriding temperature up to 500–550 °C, then the surface hardness decreases with increasing the nitriding temperature (Fig. 14b).

An inverse dependence of hardness with nitriding time was observed. A very interesting phenomenon is the relationship between the hardness of the inner layers and the γ' phase behavior, in particular, a linear increase in the inner hardness is related to an increase in the γ' phase (Fig. 15).

Residual stresses in nitride components are mainly due to the nitrides expansion into the ferrite matrix. Residual stresses are mainly governed by the nitriding temperature with a strong drop for temperatures in the range 550–600 °C (Fig. 16).

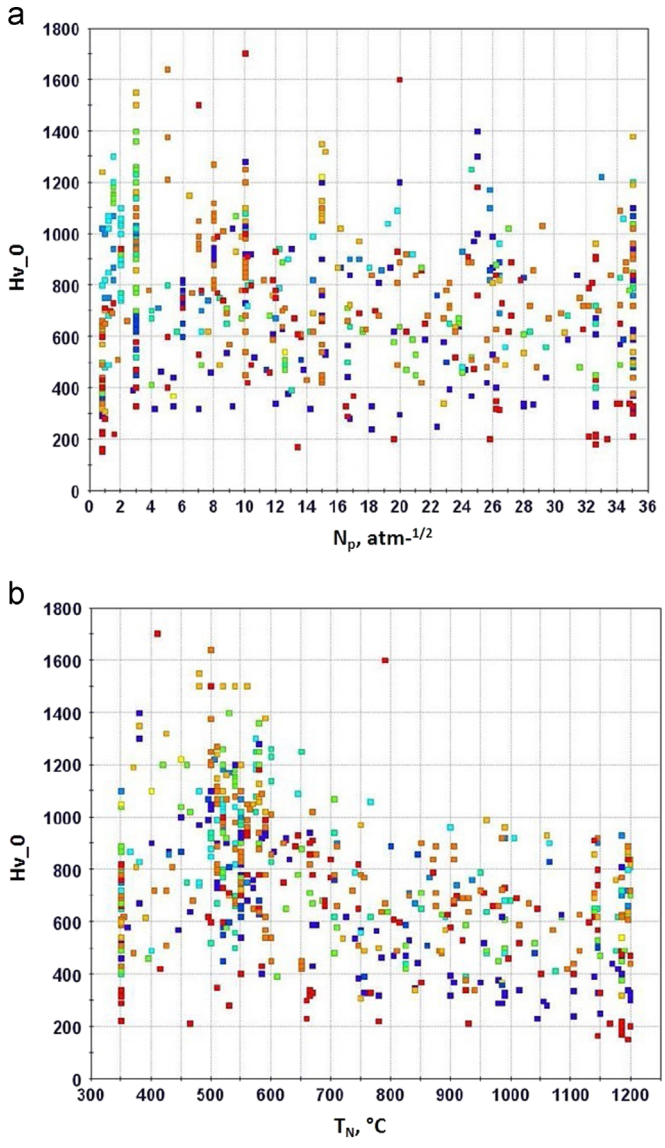

Fig. 14. Surface hardness dependence on nitrogen potential (a) and on nitriding temperature (b).

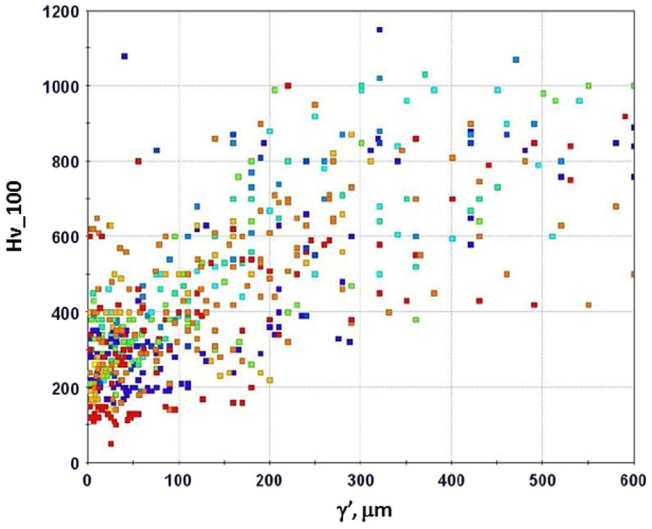

Fig. 15. Hardness dependence on γ' phase thickness.

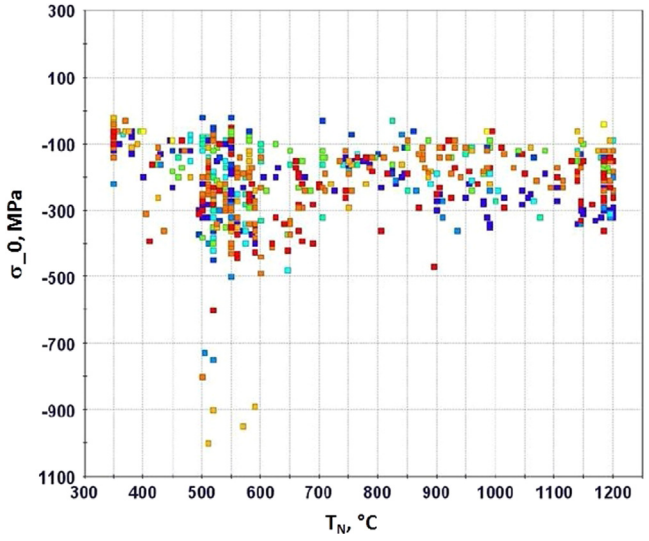

Fig. 16. Surface residual stresses dependence on nitriding temperature.

All the results provided by modeFRONTIER can be employed to develop an analytical instrument to predict the diffusional and mechanical properties of nitrided specimens. The dependence of microstructural and mechanical properties of the nitrided materials, as a function of all the employed input parameters, can be obtained. An example of such equations (Eqs. (A1)–(A5)), describing the dependences of carbon concentration, martensite phase, hardness and residual stresses at a thickness of 0.05 mm are reported in Appendix A.

3.2. Validation

The input parameters training set is underlined in Tables 4 and 5.

The validation set obtained by modeFRONTIER computing is described in Fig. 17.

Table 4
Compositional limits of the nitride steels.

Element (%)	Fe	C	Si	Cu	Mn	Cr	Ni	Mo	Al	Ti	V	Co	W
Min	63.9	0.01	0	0	0	0	0	0	0	0	0	0	0
Max	100	2.4	1.22	3	2.24	20	12	4.75	1.1	0.5	9.8	12.1	6

Table 5
Input parameters limits.

T_H (°C)	N_p (%)	T_N (°C)	t_N (h)
0	0.8	350	0.5
799	35	1200	180

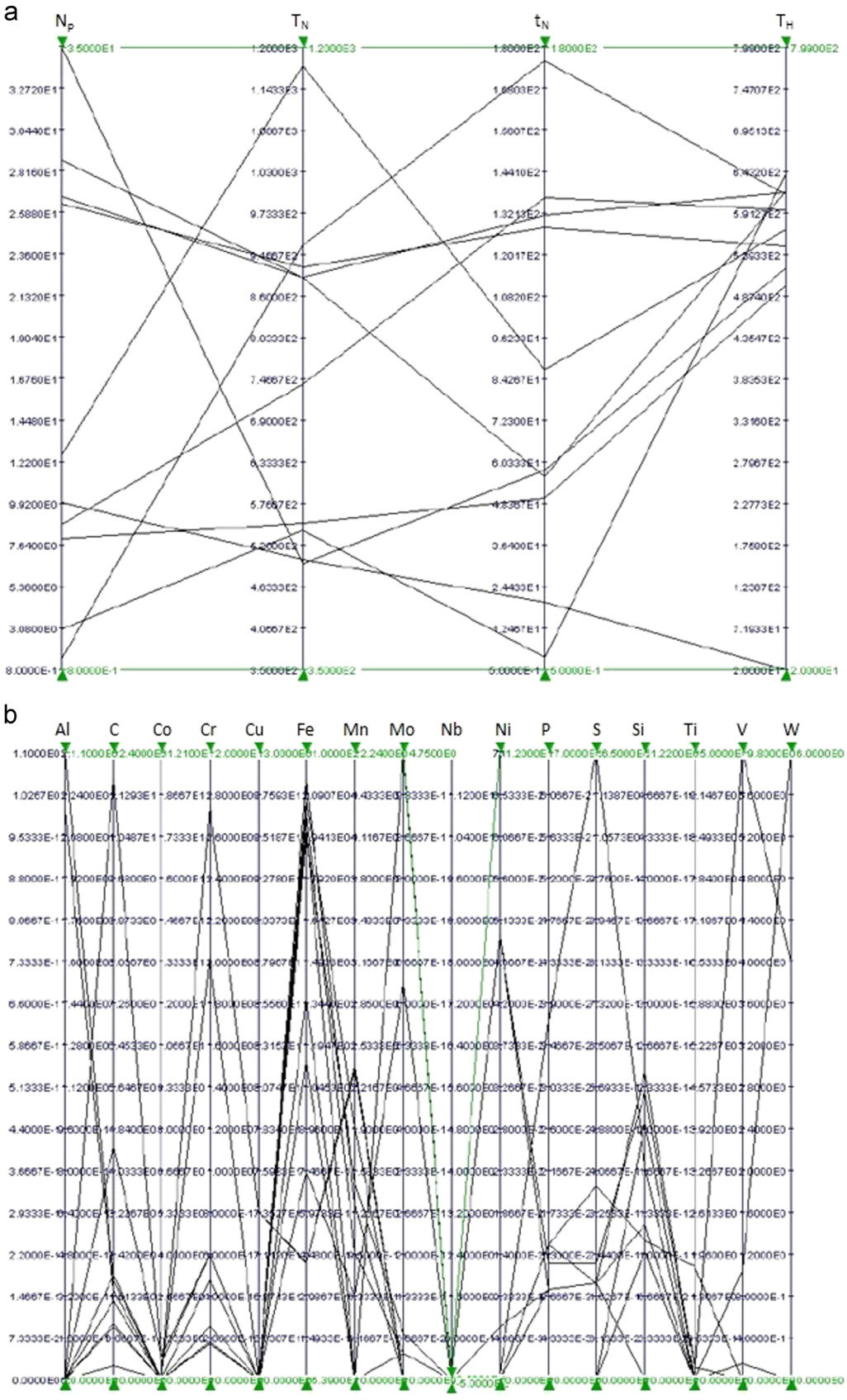

Fig. 17. Validation set as a function of nitriding conditions (a) and of steel composition (b).

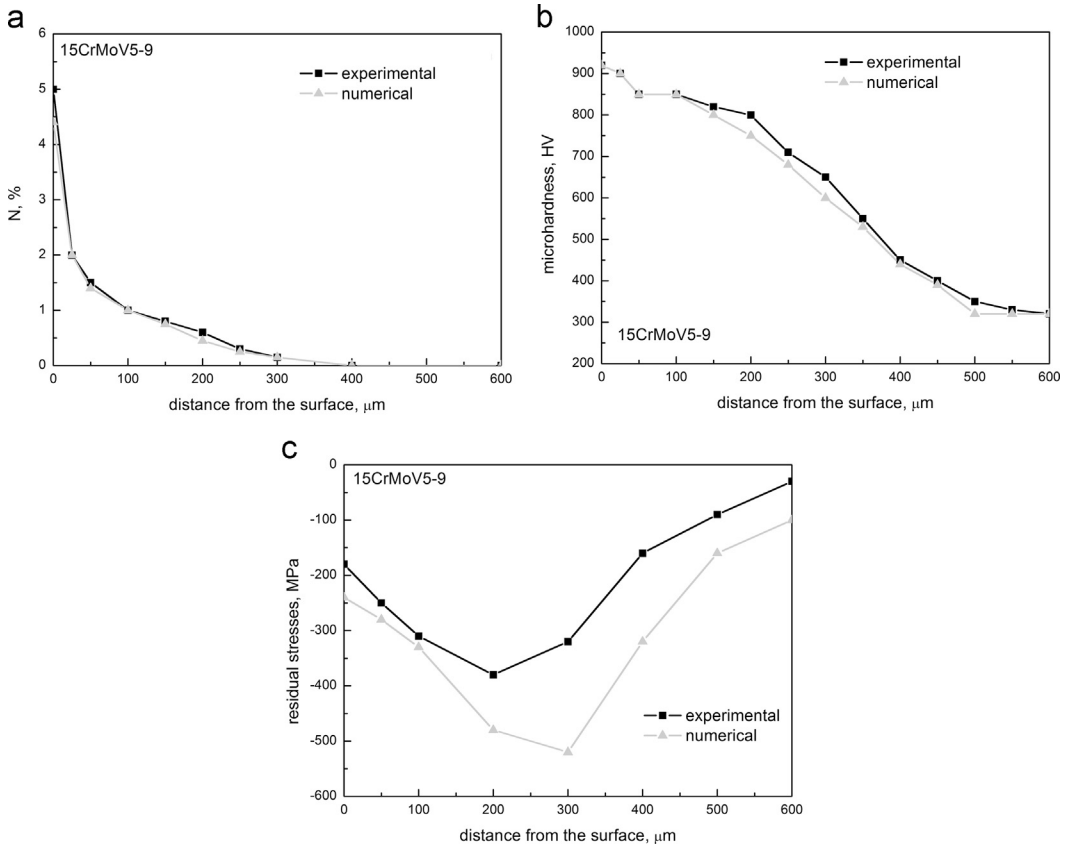

Fig. 18. Nitrogen concentration (a), microhardness (b) and residual stresses (c) as a function of the distance from the sample surface for the control design of 15CrMoV5-9 steel.

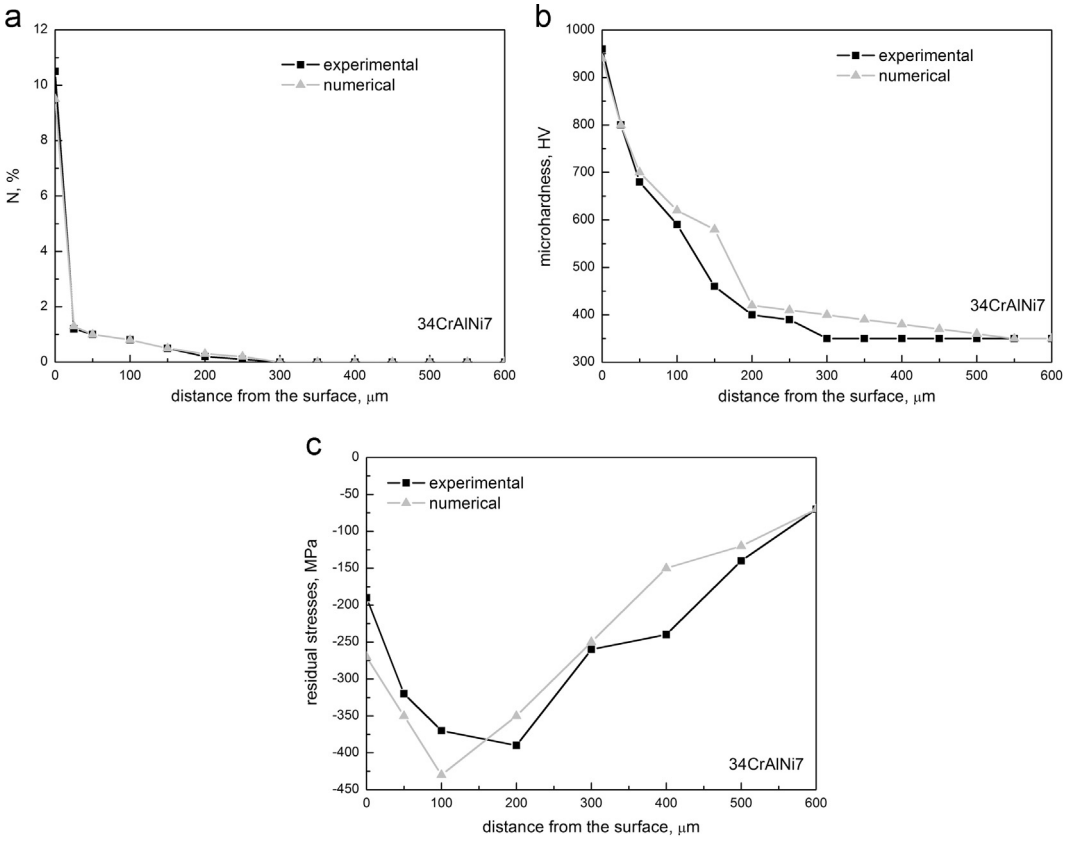

Fig. 19. Nitrogen concentration (a), microhardness (b) and residual stresses (c) as a function of the distance from the sample surface for the control design of 34CrAlNi7 steel.

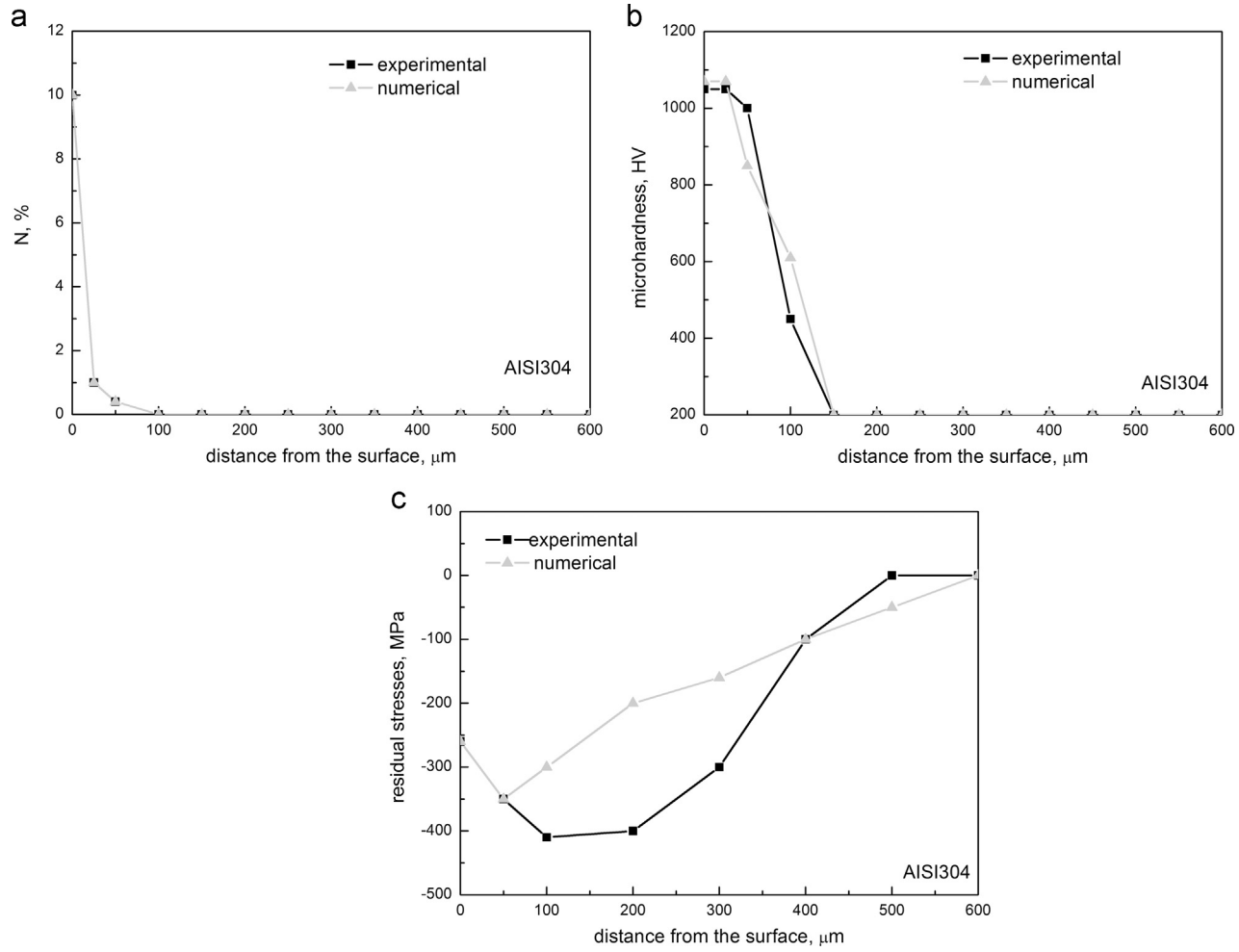

Fig. 20. Nitrogen concentration (a), microhardness (b) and residual stresses (c) as a function of the distance from the sample surface for the control design of AISI304 steel.

For the selected conditions the experimental and numerical results were compared.

The results in terms of microhardness, nitrogen profile and residual stresses of the control designs are shown in Figs. 18–21. The nitriding conditions are described in Table 4.

An excellent agreement between experimental and numerical results for the nitrogen concentration and microhardness profiles can be recorded. In some cases, such agreement differs for the residual stresses profiles (e.g. Figs. 19c and 20c). It probably depends on the range of experimental input fixed for the singular steel (e.g. AISI 304). In addition, the disagreement could be due to the employed measurement method that can be applied after the samples cut, such cut influences the residual stresses relaxation (Table 6).

For the main validation designs also the calculation of the precipitation layers thickness is in good agreement with the experimental measurements (Fig. 22). Nitriding conditions for each control design are described in Table 7.

The mean square error (MSE) applied on the points of measurement of the specific size of output was employed for the error calculation. Expressing the discrepancy between experimental and numerical values as follows:

$$\Delta y_i = y_{\exp,i} - y_{num,i} \tag{1}$$

The mean square error (MSE) for the outputs representative of a point is equal to

$$\mathrm{MSE} = \sum_{i=1}^{5} \frac{(\Delta y_i)^2}{5} \tag{2}$$

The mean square error for the 10 selected control designs is given in Table 8:

3.3. Finite element modeling (FEM) calculation and optimization

The finite element calculations were performed on cylindrical samples; the geometry is cylindrical but all the procedures can be applied to whatever kind of geometry with the only condition that the nitriding atmosphere is not stagnant (i.e. free to flow). The only requirement on the mesh is related to its refinement close to external surface: since the nitriding phenomenon affect very small thicknesses is mandatory to

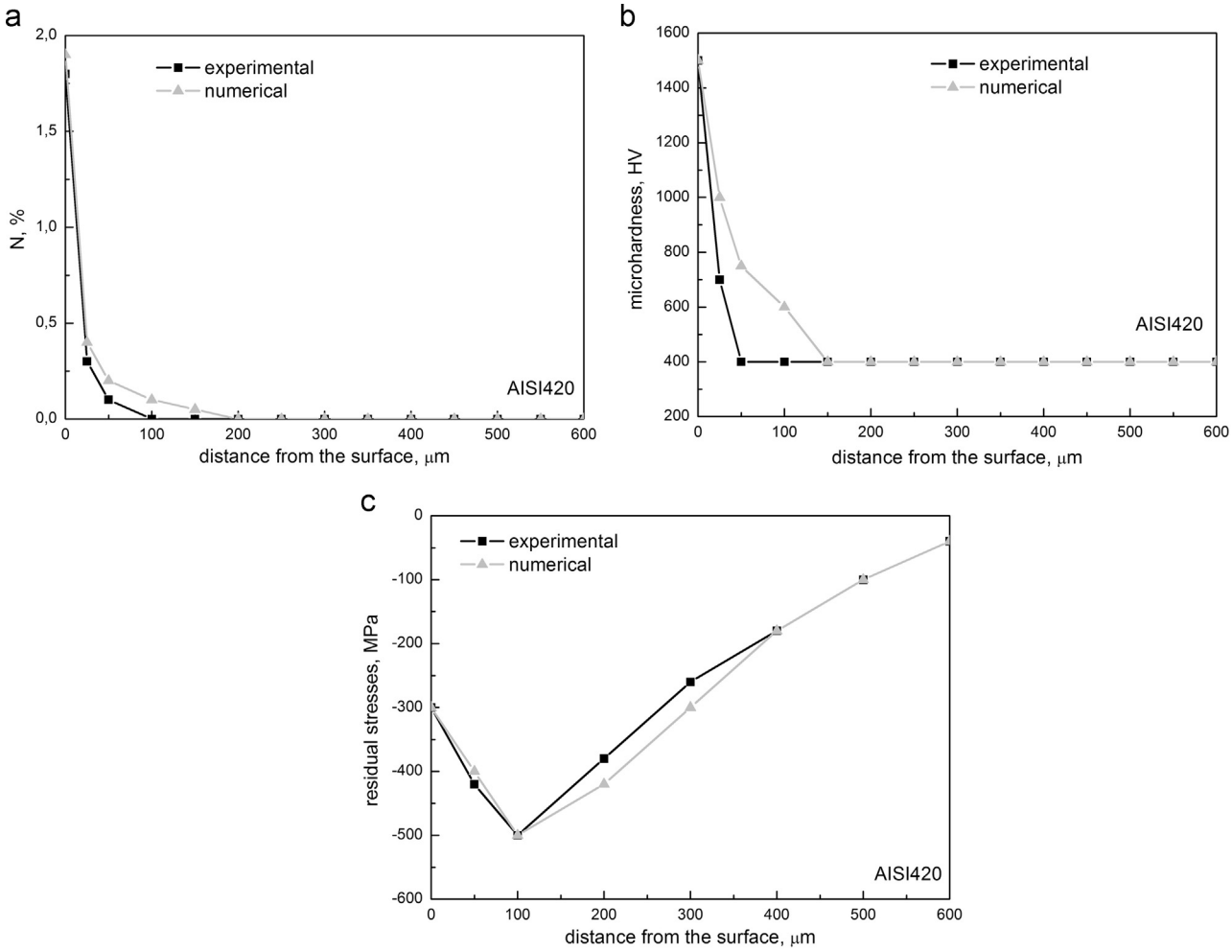

Fig. 21. Nitrogen concentration (a), microhardness (b) and residual stresses (c) as a function of the distance from the sample surface for the control design of AISI420 steel.

Table 6
Nitriding conditions for the control designs.

Steel	T_H (°C)	N_p (%)	T_N (°C)	t_N (h)
15CrMoV5-9	500	8	550	50
34CrAlNi7	550	26.4	900	128
AISI304	20	10	500	20
AISI420	640	3	540	4

build up a suitable mesh in terms of very reduced elements layers. The thickness and layer generation is driven by "inflation" option mesh for which the user has just to insert the maximum size along with the mesh which has to be more refined and the proper number of layer at the aim to describe the physical phenomena. For nitriding process the maximum penetration of N is 600 μm (Fig. 23). The Elements Type were "Solid 187", higher order 3-D, 10-node element. Convergence criterion is given by default settings, that is L2 norm with out-of-balance convergence checking (in which the difference between vector of applied loads and vector of restoring loads corresponding to the element internal loads is considered).

The material database is built by assigning the nitriding performances for each steel in terms of compositions; in this way it is possible to choose the optimal steel for each needed nitriding output and, at the end of the optimization phase, design a specific steel to reach the needed nitride conditions. In the first case it is possible to perform the simulation with fixed nitriding conditions on different steels in order to choose the best composition fitting with the needed mechanical properties. The second case is realized for those conditions with the user needs to design a new steel for very specific performances. The platform is designed to fix up to 3 objective functions in terms of mechanical properties (hardness, nitrogen concentration,

residual stresses). All the input parameters are given to the meta-models through modeFRONTIER. The post-processing of the runs is the optimization phase.

In the optimization study, different objective functions, to be related to mechanical properties to be optimized under physical constraints, are identified. The identified mechanical properties were hardness and residual stresses. By taking a look into the hardness behavior it was decided to maximize the bulk hardness, at different distances from the surface, and the surface hardness. After the convergence test, the Pareto analyses allow to identify the better compromise between the two functions. The results showed an excellent agreement for the nitrogen concentration and hardness. A more pronounced shift of numerical data from experimental ones can be underlined for the residual stresses. At the end of the analyses the hardness profiles as a function of the number of runs were identified (Fig. 24), and for those profiles the processing parameters to be employed for the achievement of the desired mechanical properties were obtained (Fig. 25).

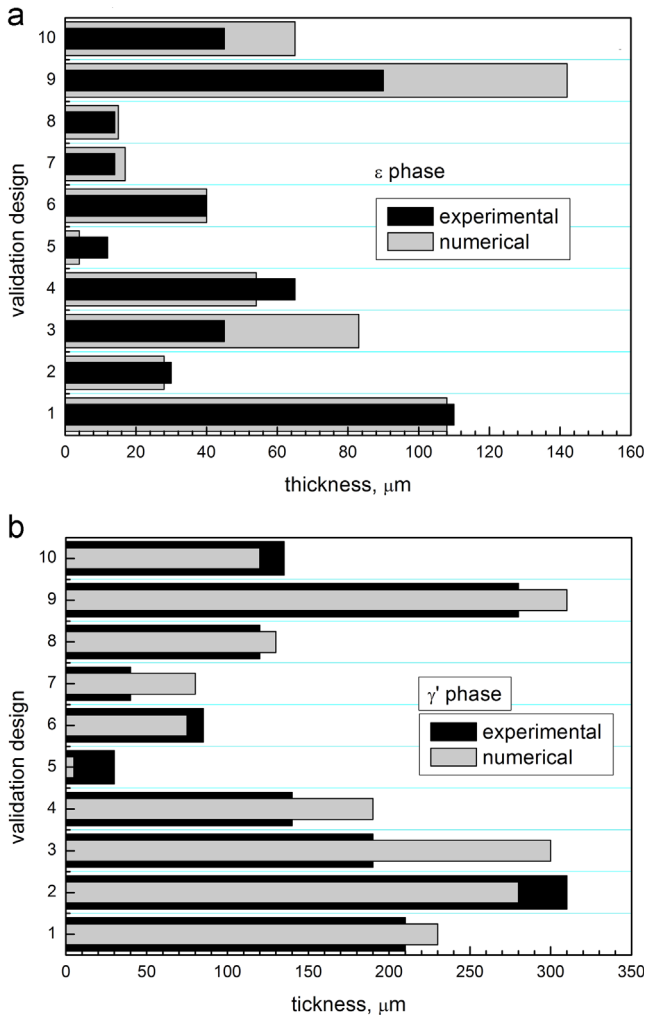

Fig. 22. Thickness comparison between numerical and experimental data for 10 control designs with regard to ε (a) and γ' (b) phases.

4. Conclusions

In the present paper experimental data, finite element calculations, and multi-objective optimization were integrated in order to develop a model capable of predicting mechanical properties, microstructural evolution and phase transformations during steel nitriding as a function of chemical compositions of steel and processing parameters. From the experimental results the mapping of nitrogen concentration, microhardness, residual stresses, and precipitate distribution as a function of different processing parameters for various steels was obtained. The results were summarized in a database useful for the further analyses, in particular to obtain the data to be compared with

Table 8
Mean square error for the nitriding output for each selected control design.

Design	N (%)	Hv (Vickers)	ε (μm)	γ' (μm)	σ (MPa)
1	0.45	19.32	0.61	18.85	69.79
2	0.18	28.15	0.58	29.60	103.7
3	1.79	97.04	38.88	111.81	85.84
4	0.33	49.07	10.12	51.66	47.81
5	1.5	83.23	7.47	35.13	61.86
6	0.07	59.62	0.33	13.43	97.84
7	0.05	134.65	2.60	35.26	24.37
8	0.28	38.53	1.3	9.33	108.99
9	0.44	35.91	51.96	17.38	46.29
10	0.45	35.21	21.19	14.49	58.33

Table 7
Nitriding conditions for the control designs.

Steel	T_H (°C)	N_p (%)	T_N (°C)	t_N (h)
AISI1020	595	8.8	740	136.5
15CrMoV5-9	500	8	550	50
31CrMo12	523	35	495	58
34CrAlNi7	550	26.4	900	128
39MoAlCr15	570	12.6	1175	87
AISI304	20.0	10	500	20
AISI420	640	3	540	4
M2	614	1.4	930	176
V2	618	28.8	885	56
18HGT	617	26.8	885	131.5

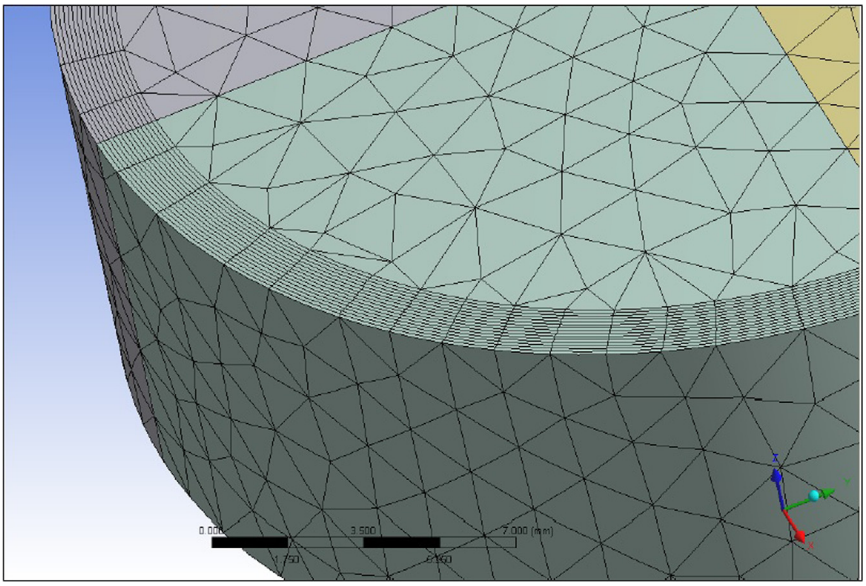

Fig. 23. Mesh geometry of the nitride samples.

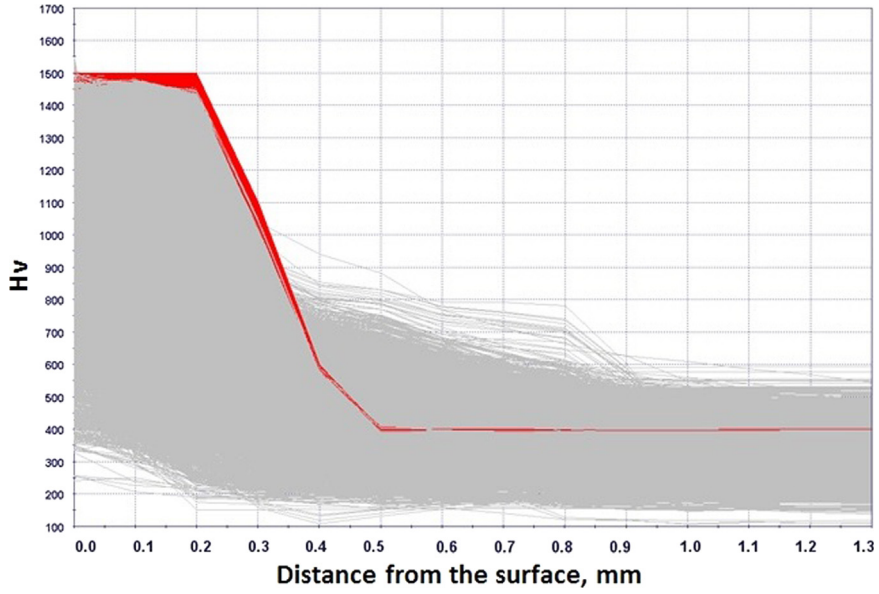

Fig. 24. Different hardness profiles as a function of the computational runs.

the numerical ones. From the analyses of the correlation matrixes it was calculated that nitrogen concentration on the surface is strongly dependent on nitrogen potential and on nitriding time then on nitriding temperature with different weights; surface hardness is dependent strongly on nitriding temperature then on nitrogen potential with different weights; residual stresses on the surface are dependent on the nitrogen potential while the residual stresses in the inner layers are dependent on nitriding temperature; residual stresses are strongly function of the compound layers formed during diffusion. A deep local analyses allowed to calculate the dependence of mechanical and microstructural behavior, at fixed distances from the surface, on all the employed experimental processing parameters. All the data were employed for the calculation and optimization through modeFRONTIER and ANSYS in order to develop an analytical instrument capable of predicting the microstructure and mechanical properties of steels during nitriding in a broad range of conditions. In particular, a generalized solution of Fick's law was obtained and the equations relating microstructural and mechanical properties (nitrogen concentration, nitrides layers, microhardness and residual stresses) of different steels as a function of nitriding parameters were calculated. The calculations led to the definition of the independent coefficients solved by ANSYS through modeFRONTIER my matching in closed loops the solutions with the experimental data. In the validation phase, the correlation between experimental and numerical results (obtained by the previous described procedure) was

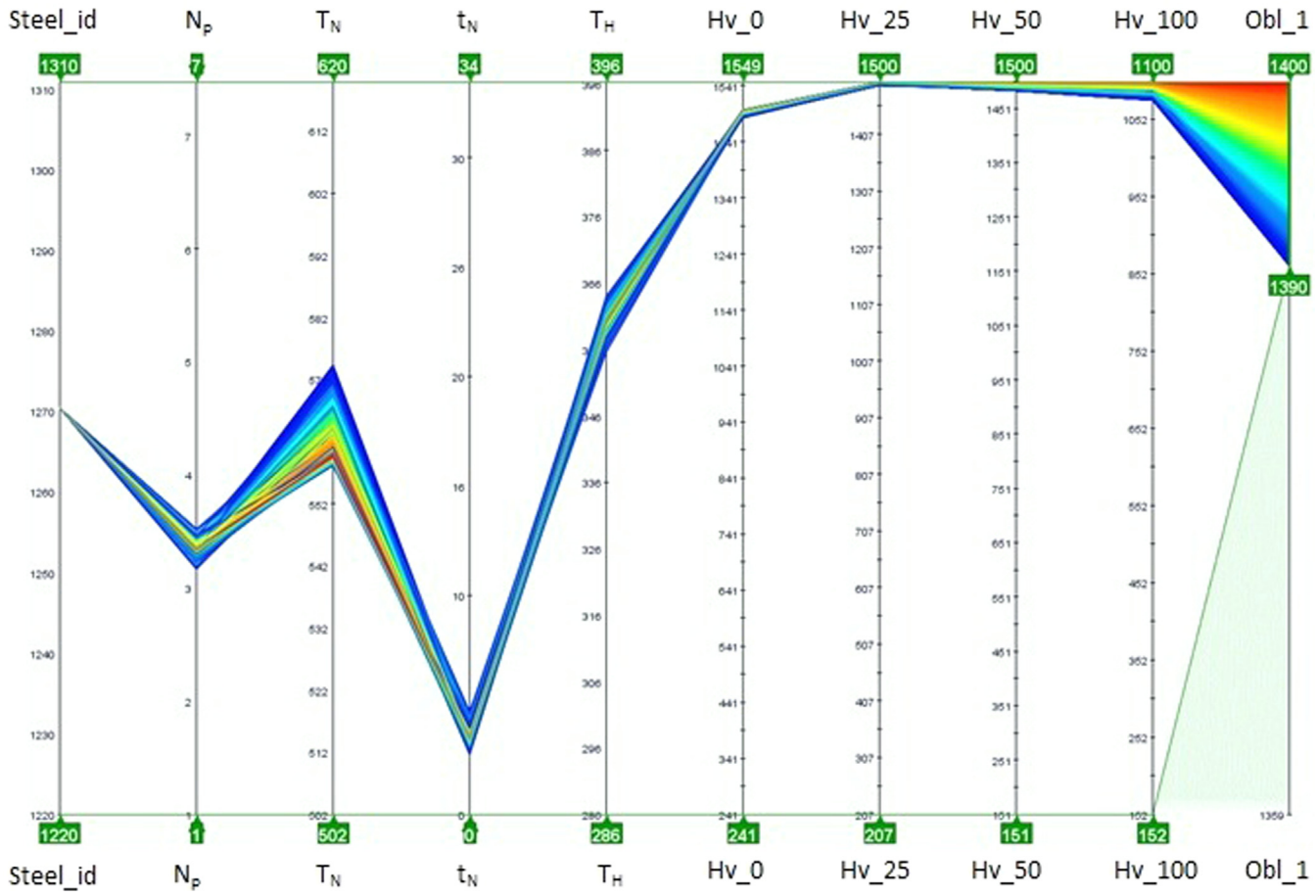

Fig. 25. Processing parameters chart for the optimized hardness profiles.

analyzed for selected control design belonging to AISI1020, 15CrMoV5-9, 31CrMo12, 34CrAlNi7, 39MoAlCr15, AISI304, AISI420, M2, V2, 18HGT steel. At the end of the study different designs were identified optimized to achieve the maximization of surface and bulk hardness of the nitrided steel.

Conflict of interest

The authors do not have any conflict of interests.

Acknowledgments

The authors gratefully acknowledge ENGINSOFT S.p.A. for the technical support and the PUGLIA REGION for the findings provided to the project S.T.A.R.-EXD (Simulation Technology Aeronautic Research-Extended Data) in the program action F.E.S.R. sul P.O. Regione Puglia 2007–2013, Asse I-Linea 1.1 – Azione1.1.2. Aiuti agli Investimenti in Ricerca per le PMI".

Appendix A

N_0 = 1.1264495247462203 + ((((cos(((1 × (Mn + ln(N_p)))/cos((exp(Cr) × (Ti × exp(Cr)))))) + (cos((cos((Ti × exp(t_N))) + ((exp(Ti) × ln(T_N)) + ln(N_p)))) + (Mn + ln(N_p)))) × cos((exp((ln(t_N) × ((Mn + ln(N_p)) × sin(V))))/t_N))) − cos((((cos((Ti × exp(N_p)))t_N) + ((ln(N_p)/cos((Ti × exp(N_p))))/cos((Ti × (Ti × exp(N_p)))))) × cos(exp(((Mn + Mn)/cos((1 × sin(Mn))))))))) + ((((((Ti + ln(N_p)) × cos((ln(N_p)/t_N))) × cos((cos((Ti − ln(T_N)))/t_N))) − cos(((((C + exp(Ti)) × (Ti + ln(N_p))) × cos((Ti × exp(N_p)))) × cos(((Mn + ln(N_p)) + sin(V))))) × cos((((Co × cos(N_p)) × cos(N_p)) × cos((ln(N_p) × cos((Ti × Si)))))) − cos(exp(((Mn + Mn)/cos((V × cos((Co-Mn))))))))

Equation A1: Nitrogen concentration on the samples surface as a function of processing parameters and steel composition.

N_200 = −0.8191165912391943 + (cos(sin(ln(((T_N + ((((V × exp(Mn)) × (W × cos(T_N))) − (N_p/cos(W))) × (((V + exp(Mn)) + cos(exp(Mn))) − sin(((V + T_N)/Fe)))))))) + ((((V/Fe)/exp(sin(sin(cos(W)))))/exp((Al × ((((T_N + V) + T_N)/((cos(T_N) + cos(T_N)) − ln((V + T_N)))))))/sin(ln(((T_N + ((V/cos(T_H)) × exp(Mn))) + ((((V/cos(C)) + (exp(Mn)/cos(T_H))) + (exp(Mn)/cos(T_H))) + (exp((cos(T_N) + cos(T_N))) × cos(T_H))))))))

Equation A2: Nitrogen concentration at a distance of 200 μm from the nitride surface as a function of processing parameters described into nomenclature and alloying elements.

HV_0 = 1202.6242028807285 + ((((((((((Cr/0.1) − (V/0.1)) − (Fe/(Mo + t_N))) − (((V/0.1) + 0.1) + (Ni + t_N))) − (Fe/((Al/0.1) + N_p))) − ((Fe − ((Al − (T_N/10)) + 1))/(Cr + ((V/0.1) + 1)))) − (Fe/((Mo/(((Cr + 1)/(V + t_N))/(W + (W + t_N))))) + ((V/0.1) + 1)))) − ((Fe − (((Cr/0.1) − (Fe/((V/0.1) + 1))) + 1))/((V/

((Cr+t_N)/((Fe/10)+((Cr+1)−(V/0.1)))))+(((Al/(10/(t_N+t_N)))+Mn)+1)))−(((Fe−(((Cr/0.1)−(Fe/((V+t_N)+1)))+Mo))/((V/((((Cr+1)−(V/0.1))−(Fe/(Cr+1)))−((10/(V+t_N))+(W+t_N))))+(((((Cr/0.1)/(W−Fe))/((Fe/t_N)/0.1))+Mn)+1)))/((V/(((Al/(10/(W+Fe)))−(Fe/(S−(T_N/10)))))−((Fe/(Cr+t_N))+((10/(Fe/t_N))/(C+(Cr+1))))))+((((Al/(10/(0.1+t_N)))/((10/(V+t_N))/(W+(Al+t_N))))+(Mo/((10/(V+t_N))/(10/(Cr+1)))))+1))))−(T_N/(Fe/((((Cr+1)+10)+V)+10))))

Equation A3: Hardness concentration on the samples surface as a function of processing parameters described into nomenclature and alloying elements.

$\mathbf{e}_f$ = −279.8784048207975+((((cos((((ln(T_N)−0.1)+((Mn−S)/(ln(T_N)−exp(C))))+(((Ti−0.1)−0.1)+(ln(T_N)+(ln(T_N)+ln(T_N))))))×(ln((((t_N+exp(exp(C)))+(((Mn−S)−exp(1))−Mo)))+(((exp(C)−Si)−0.1)−0.1)))+(cos(((ln(T_N)−((Mn−S)/(Mn−0.1)))+(ln((ln(T_N)−(Mn−Ni)))+((ln(T_N)+Ni)+(ln(T_N)+ln(T_N))))))+(((((ln(T_N)−0.1)+((Mn−S)/(Mn−0.1)))+((ln(T_N)−Si)+Al))+(Al+(((Mn−0.1)−0.1)+(ln(T_N)+ln(T_N)))))+(ln((t_N+exp(exp(C))))+(exp(C)−Si)))))/0.1)−(((exp(C)+((cos(T_N)+(exp(C)/(((Mn−S)/(Mn−0.1))−exp(C))))+(exp(C)/(((Mn−S)/(Mn−0.1))−exp(C)))))/(ln((((ln(T_N)−(Mn−S))+exp(1))−(Mn−S)))+(((((Mn−S)/(Mn−0.1))−exp(C))−0.1)+(ln(T_N)+Ni))))+(((((((Mn−0.1)+(ln(T_N)+ln(T_N)))+(ln(T_N)+ln(T_N)))+(Al+((ln(T_N)−Si)+(ln(T_N)+ln(T_N)))))+(ln((t_N+exp(ln(T_N))))+((cos(T_N)+(ln(T_N)+ln(T_N)))−Si)))/((((ln(T_N)−0.1)−0.1)−0.1)−((Mn-S)/(((Mn-S)/(Mn-0.1))−exp(C)))))+Ni)))

Equation A4: Thickness of the ε nitrides as a function of processing parameters described into nomenclature and alloying elements.

$\mathbf{g'}_f$ = 98.68824774543444+(((Fe−((((((T_N×0.1)−(sin((V×10))×10))−((sin(ln(T_N))×10)×10))−(sin(((((T_N×0.1)−ln(T_H))/ln(T_H)))×(ln(t_N)×10)))−(Co-((((((T_N×0.1)−(V-N_p))−(ln(t_N)×10))−(ln(t_N)-N_p))−(Al×((ln(t_N)×ln(T_N))−ln(T_H)))))))+((S−((((((Mn/N_p)+Fe)−((Mn-Si)−(T_N×0.1)))−((T_N×0.1)−10))−(ln(T_H)×ln(T_N)))−(Al×((ln(t_N)×(ln(t_N)×10))−((((T_N×0.1)−(Mn-Si))−(ln(t_N)×ln(T_N)))))))/N_p))−((((((((T_N×0.1)−((Mn-Si)×10))−((sin(ln(T_N))×10)×10))−(((((T_N×0.1)−10)/(S−10))/(S−10)))×ln(10))−((sin(((((T_N×0.1)−10)/((ln(T_H)×ln(T_N))−10)))×(ln(t_N)×10))−(((((((T_N×0.1)−ln(T_N))−(ln(t_N)×ln(t_N)))−((V×10)+Fe))−((Mn-Si)×Cr))−Fe)))−((sin(((((T_N×0.1)−10)/((ln(T_H)×ln(T_N))−10)))×(sin(((((T_N×0.1)−10)/(S-10)))×(ln(t_N)×10)))+((Al/(((((S-Fe)−ln(T_N))−N_p)−(((T_N×0.1)−ln(T_H))−((+p_Fe)))−Ni))−((((((T_H×P)−(V×10))−0.1)−(V+10))−(sin(((((T_N×0.1)−10)/(S−10)))×(ln(t_N)×10)))))))

Equation A5: Thickness of the γ' nitrides as a function of processing parameters described into nomenclature and alloying elements.

References

[1] Cavaliere P, Zavarise G, Perillo M. Modeling of the carburizing and nitriding processes. *Computational Materials Science* 2009;**46**(1)26–35.

[2] Mittemeijer EJ, Somers MAJ. Thermodynamics, kinetics, and process control of nitriding. *Surface Engineering* 1997;**13**(6)483–97.

[3] Appolaire B, Gouné M. Linear stability analysis of a γ′-Fe4N nitride layer growing in pure iron. *Computational Materials Science* 2006;**38**(1) 126–35.

[4] Keddam M, Djeghlal ME, Barrallier L, Salhi E. Computer simulation of nitrided layers growth for pure iron. *Computational Materials Science* 2004;**29**(1)43–8.

[5] Torchane L, Bilger P, Dulcy J, Gantois M. Control of iron nitride layers growth kinetics in the binary Fe–N system. *Metallurgical and Materials Transactions A* 1996;**27A**:1823–34.

[6] Dimitrov VI, D'Haen J, Knuyt G, Quaeyhaegens C, Stals LM. Modeling of nitride layer formation during plasma nitriding of iron. *Computational Materials Science* 1999;**15**(1)22–34.

[7] Akhtar SS, Arif AFM, Yilbas BS. Evaluation of gas nitriding process with in-process variation of nitriding potential for AISI H13 tool steel. *International Journal of Advanced Manufacturing Technologies* 2010;**47** (5–8)687–98.

[8] Özdemir B, Lippmann N. Modeling and simulation of surface reactions and reactive flow of a nitriding process. *Surface & Coatings Technology* 2013;**219**:151–62.

[9] Peng DQ, Kim TH, Chung JH, Park JK. Development of nitride-layer of AISI 304 austenitic stainless steel during high-temperature ammonia gas-nitriding. *Applied Surface Science* 2010;**256**:7522–9.

[10] Kong JH, Lee DJ, On HY, Park SJ, Kim SK, Kang CY, Sung JH, Lee HW. High temperature gas nitriding and tempering in 17Cr1Ni0.5C0.4V steel. *Metals and Materials International* 2010;**16**:857–63.

[11] Lee HW, Kong JH, Lee DJ, On HY, Sung JH. A study on high temperature gas nitriding and tempering heat treatment in 17Cr–1Ni–0.5C. *Materials and Design* 2009;**30**:1691–6.

[12] Hassani-Gangaraj SM, Guagliano M. Microstructural evolution during nitriding, finite element simulation and experimental assessment. *Applied Surface Science* 2013;**271**:156–63.

[13] Kochmanski P, Nowacki J. Influence of initial heat treatment of 17-4 PH stainless steel on gas nitriding kinetics. *Surface & Coatings Technology* 2008;**202**:4834–8.

[14] Kurz SJB, Meka SR, Schell N, Ecker W, Keckes J, Mittemeijer EJ. Residual stress and microstructure depth gradients in nitrided iron-based alloys revealed by dynamical cross-sectional transmission X-ray micro-diffraction. *Acta Materialia* 2015;**87**:100–10.

[15] Keddam M, Bouarour B, Kouba R, Chegroune R. Growth kinetics of the compound layers: effect of the nitriding potential. *Physics Procedia* 2009;**2**:1399–403.

[16] Akhtar SS, Fazal A, Arif M, Yilbas BS. Influence of multiple nitriding on the case hardening of H13 tool steel: experimental and numerical investigation. *International Journal of Advanced Manufacturing Technology* 2012;**58**:57–70.

[17] Arif AFM, Akhtar SS, Yilbas BS. Effect of process variables on gas nitriding of H13 tool steel with controlled nitriding potential. *International Journal of Surface Science and Engineering* 2010;**4**:396–415.

[18] Ju H, Li LX, Wang QB, Diao JP. Optimum design of the gas nitriding technological parameters of H13 steel. *Gongneng Cailiao/Journal of Functional Materials* 2011;**42**:405–7.

[19] Yang M, Zimmerman C, Donahue D, Sisson Jr. RD. Modeling the gas nitriding process of low alloy steels. *Journal of Materials Engineering and Performance* 2013;**22**:1892–8.

[20] Yang M, Sisson Jr. RD. Modeling the nitriding process of steels. *Advanced Materials and Processes* 2012;**170**:33–6.

[21] Williamson GK, Hall WH. X-ray line broadening from filed aluminium and wolfram. *Acta Metallurgica* 1953;**1**(1)22–31.

[22] Cavaliere P, Perrone A, Silvello A. FEM and milti-objective optimization of steel case hardening. *Journal of Manufacturing Processes* 2015;**17**: 9–27.